Meteorologische Zeitschrift, PrePub DOI 10.1127/metz/2016/0773

Statistical-dynamical downscaling of the urban heat island in Hamburg, Germany

Peter Hoffmann[1,2*], Robert Schoetter[2,3] and K. Heinke Schlünzen[2]

[1]Department of Mathematics, University of Hamburg, Hamburg, Germany
[2]Meteorological Institute, University of Hamburg, Hamburg, Germany
[3]CNRM-GAME, Meteo France, Toulouse, France

(Manuscript received January 8, 2016; in revised form August 22, 2016; accepted October 5, 2016)

Abstract

Regional climate models provide climate projections on a horizontal resolution in the order of 10 km. This is too coarse to sufficiently simulate urban climate related phenomena such as the urban heat island (UHI). Therefore, regional climate projections need to be downscaled. A statistical-dynamical method for the UHI was developed and applied to provide urban climate results at a high resolution with little computational costs. For the downscaling, weather situations relevant for the UHI are determined. This is done by combining objective weather pattern classification based on a k-means cluster analysis of ERA-40 reanalysis data and a regression-based statistical model of the observed UHI of Hamburg. The resulting days for each weather pattern are simulated with the mesoscale meteorological model METRAS at 1 km horizontal resolution. To obtain the average UHI for a climate period, the mesoscale model results are statistically recombined weighted by the frequency of the corresponding weather patterns. This is done for present-day climate (1971–2000) using reanalysis data to yield the current climate UHI. For the future climate periods 2036–2065 and 2070–2099 the results of regional climate projections are employed. Results are presented for Hamburg (Germany). The present day UHI pattern is well reproduced compared to temperature data based on floristic mapping data. The magnitude of the early night-time UHI is underestimated when compared to observed minimum temperature differences. The future UHI pattern does only slightly change towards the end of the 21st century based on A1B scenario results of the RCMs REMO and CLM. However, for CLM the number of days with high UHI intensities significantly increases mainly due to a decrease in near-surface relative humidity.

Keywords: downscaling, statistical-dynamical downscaling, climate modelling, numerical model, weather pattern, urban heat island

1 Introduction

Regional climate projections are currently available at about 10 km horizontal resolution (e.g. Jacob et al., 2008, Katzfey et al., 2016). For the development of climate change adaptation strategies for urban areas, characterizing the urban heat island (UHI) is important because its magnitude (up to 10 K under optimal conditions; Yow, 2007; ~2.5 K in the summer average for minimum temperature differences in Hamburg at densely build-up sites and 0.5 to 1 K in suburban areas; Schlünzen et al., 2010) can be locally much higher than the projected temperature changes due to climate change (2–3 K for Northern Germany at the end of the 21st century assuming the A1B scenario; Daschkeit, 2011). Since the UHI cannot be resolved by ~10 km grids regional climate projections need to be further downscaled.

Downscaling methods can be grouped into three main types: statistical, dynamical and statistical-dynamical downscaling. For statistical downscaling, a statistical relationship between large-scale variables simulated by a coarser model and a small scale variable is established (Wilby and Wigley, 1997). Statistical downscaling has been successfully applied to investigate changes of the UHI intensity (Wilby, 2003; Wilby, 2008; Hoffmann et al., 2012). Using this technique, the spatial pattern of the UHI can hardly be obtained, in particular if there are only few sites with observational data available. This is a major drawback when planning climate change adaptation measures for cities because spatial information is needed. Also the impact of adaptation measures on the UHI can hardly be quantified when using a statistical downscaling technique.

To dynamically downscale a regional climate projection to a horizontal grid of about 1 km for a 30-year period is computationally expensive, especially if the simulations need to be repeated several times in order to quantify the impact of different adaptation measures. Hamdi et al. (2014, 2015) use dynamical downscaling to refine climate model simulations to a resolution of 4 km. They further use the near-surface meteorological variables at 4 km resolution to force an urban surface scheme at 1 km horizontal resolution. However, this "offline" approach neglects the interactions between

*Corresponding author: Peter Hoffmann, Department of Mathematics, University of Hamburg, Bundesstraße 55, 20146 Hamburg, Germany, peter.hoffmann@uni-hamburg.de

the finer resolved surface and the coarser meteorological forcing. To overcome the disadvantages of the first mentioned methods, statistical-dynamical downscaling (SDD) can be applied (Frey-Buness et al., 1995). The SDD method makes use of the ability of climate models to simulate the large-scale circulation better than small-scale processes and assumes that the small-scale meteorological variable (e.g. the near-surface temperature, precipitation) depends on large-scale weather pattern (WP). High-resolution numerical model simulations are then to be performed for each WP. To calculate the climatological average, the simulation results are statistically recombined by weighting with the frequency of the WPs. The change of the small-scale variable in future climate is determined by the change in the frequency of the WPs. SDD methods have been applied to variables such as temperature (Fuentes and Heimann, 2000), precipitation (Huebener and Kerschgens, 2007a,b), and wind speed (Pinto et al., 2010; Najac et al., 2011). Najac et al. (2011) extended the SDD-concept and introduced within WP variations in the statistical part of the SDD method. For urban climate, a simple SDD method has been applied by Früh et al. (2011a,b). The statistical part of their method is not based on WPs but on prescribed linear combinations of temperature, wind speed and relative humidity. The extremes of these variables are used as initial values to conduct idealized simulations with a mesoscale model without nesting. The simulation results are statistically recombined using the so-called cuboid method to downscale RCM results with respect to urban heat load in the Frankfurt am Main area. Due to the simple treatment of the flow conditions (only two wind directions), the temperature pattern might be unrealistic because the advection of the UHI is not considered properly. In addition, no large-scale changes of the forcing data are considered in any of the simulations.

Apart from the study of Hamdi et al. (2014, 2015), numerical studies of the UHI usually focus on idealized meteorological conditions (e.g. Atkinson, 2003, Früh et al. 2011a,b) or on days with anticyclonic conditions (e.g. Flagg, 2010; Bohnenstengel et al., 2011; Grawe et al., 2012). However, such meteorological conditions are rare for many cities. It is also questionable whether only the maximum UHI is of interest, because it might occur at days where the UHI is less important from the point of view of adaptation to climate change, because the prevailing air temperature is neither very high (risk of tropical night/ heat stress) nor very low (risk of frost). Hoffmann and Schlünzen (2013) showed that high UHI values also occur for WPs different from those considered in previous studies. Hence, simulating only anticyclonic meteorological situations might not result in a realistic UHI pattern. Thus, weather situations that are resulting in large UHI values need to be determined. Hoffmann and Schlünzen (2013) constructed a weather pattern classification (WPC) to explain variations in Hamburg's UHI intensity and obtained 7 WPs for the summer months. However, these WPs only account for a small part of the UHI variance because of the low number of WPs and the dependency of the UHI on small-scale variables. Hence, further information is needed to subdivide the WPs according to the strength of the UHI intensity.

The aim of this study is to construct and apply a SDD method to downscale regional climate projections to a final resolution of 1 km. For this, weather patterns are determined that have different characteristics and relevance for the UHI intensity. The SDD method is described in detail in Section 2. Section 3 introduces the RCM data that are used for the SDD method. The setup of the dynamical simulations that are performed for the area of Hamburg is presented in Section 4. The results for current and future climate are given in Section 5, concluding remarks in Section 6.

2 Statistical-dynamical downscaling method

The SDD method applied in this study is schematically presented in Fig. 1. The method aims at determining the mean seasonal spatial pattern of the nocturnal UHI. For each season, WPs are determined that represent the UHI's day-to-day variability. The focus is on the area of Hamburg, the clustering method is described by Hoffmann and Schlünzen (2013). The UHI variance explained by this WPC is too small to only simulate the days which are closest to the cluster centers. This is mainly due to the intended low number of WPs. Usually, the number of WPs used for SDD methods is higher. Fuentes and Heimann (2000) used 22, Pinto et al. (2010) used 55. However, the choice of the number of WPs is purpose driven and for this study a larger number of WPs is not optimal, because some of the resulting WPs could be too similar. This would lead to problems when detecting the WPs in different RCMs. Therefore, an approach similar to Najac et al. (2011) is used. They selected multiple non-consecutive days within one WP for their simulations. Their selection was based on 850 hPa u- and v- wind components. The WPs were subdivided according to the strength of the 850 hPa wind field. Instead of taking the strength of a certain classification variable, an estimate for the strength of the daily UHI intensity within each WP is used in the present study. Since this estimate has to be calculated for both the current and the future climate, the observed UHI cannot be used. Instead a statistical model for the UHI, similar to that used by Hoffmann et al. (2012), is constructed. Using a multiple linear regression (2.1), the UHI is described as a linear function of the daily averaged values for wind speed FF, cloud cover of the previous day CC, and relative humidity RH.

$$\Delta T_{u-r} = aFF + bCC + cRH + d \qquad (2.1)$$

ΔT_{u-r} denotes Hamburg's UHI, described as the difference of the daily minimum temperature measured at the German Meteorological Service's (DWD) urban station Hamburg-St. Pauli and the average of the minimum

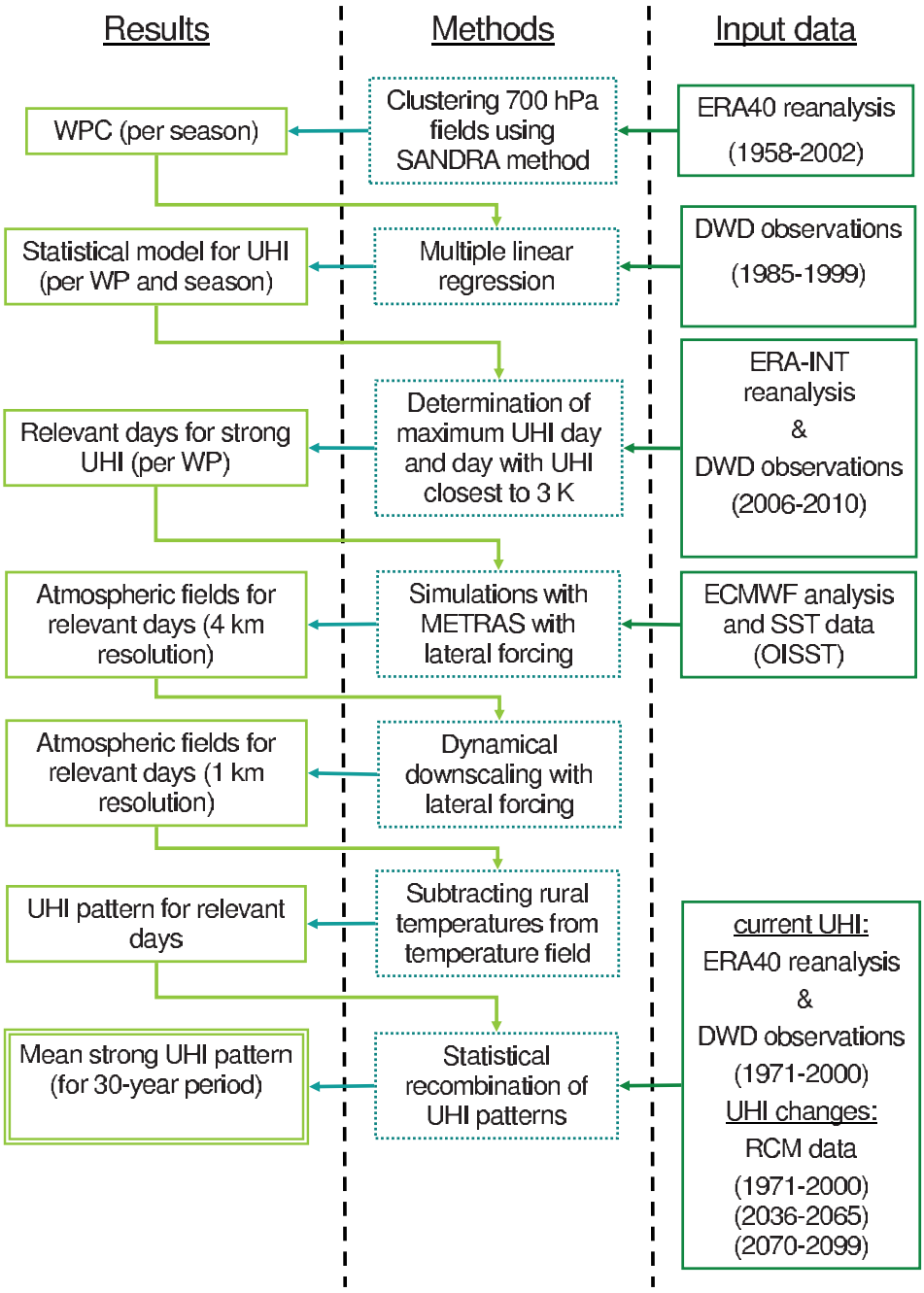

Figure 1: Schematic diagram of the statistical-dynamical downscaling method for Hamburg's UHI. Results are indicated by light green boxes, methods dashed green boxes and the input data by solid dark green boxes.

temperatures observed at the rural DWD stations Grambek (GR) and Ahrensburg (AH). Different to Hoffmann et al. (2012) data for all variables of the statistical model (*FF*, *CC*, *RH*) are taken from the DWD climate reference station Hamburg-Fuhlsbüttel (FU) in the present study because of its long and continuous time series. It should also be noted that St. Pauli station is chosen since it shows the largest UHI of all DWD sites in Hamburg based on minimum temperature differences. The statistical model parameters a, b, c, and d are computed for each WP separately. Therefore, different statistical relationships result for the WPs. This combination of the WPC and statistical model explains about 50 % of the UHI variance with a root-mean-square error of about 1.2 K.

By combining the WPC with the statistically modelled ΔT_{u-r}, the "relevant days" can be determined. A "relevant day" is defined as a day with a strong UHI intensity, because these days are of largest interest for planning climate change adaptation measures. A simulation of days with weak UHIs would lead to an unnecessary increase in computational cost. Therefore, a threshold UHI intensity $(\Delta T_{u-r})_{\mathrm{Thres}} = 3\,\mathrm{K}$ is introduced. All days with $\Delta T_{u-r} \geq (\Delta T_{u-r})_{\mathrm{Thres}}$ are then considered as strong UHI days. The chosen threshold leaves 25 % of the summer days within the data sample. This means

Table 1: Surface characteristics for the 36 surface cover classes with Albedo α_0, thermal diffusivity k_s, thermal conductivity ν_S, soil water availability (initial values) α_q, saturation value for soil water content W_K, and roughness length z_0.

Surface cover class	α_0	k_s [m^2/s]	ν_S [W/mK]	α_q	W_K [m]	z_0 [m]
water	0.10	1.50E-07	100.00	0.98	100.000	$f(u_*)$
water, fresh, stationary	0.10	1.50E-07	100.00	1.00	100.000	$f(u_*)$
water, fresh, dynamic	0.10	1.50E-07	100.00	1.00	100.000	$f(u_*)$
water, salty	0.10	1.50E-07	100.00	0.98	100.000	$f(u_*)$
mudflats	0.10	7.40E-07	2.20	0.98	100.000	0.0002
ground, bare	0.17	3.80E-07	1.18	0.30	0.015	0.0012
sand	0.20	5.70E-07	1.05	0.10	0.010	0.0003
gravel	0.12	2.76E-07	0.40	0.10	0.010	0.0050
sand dune, with grass	0.20	5.70E-07	1.05	0.15	0.035	0.0100
sand dune, with sparse vegetation	0.20	5.70E-07	1.05	0.15	0.045	0.0500
asphalt	0.09	2.30E-06	1.35	0.50	0.002	0.0003
brick/pavers	0.30	2.30E-06	0.90	0.02	100.000	0.0006
Steel	0.30	4.20E-06	30.00	0.50	0.001	0.0003
bushes, on wet soil	0.20	5.20E-07	1.33	0.65	100.000	0.1000
ground, bare, on wet soil	0.17	7.40E-07	2.20	0.60	100.000	0.0012
grass, short, on dry soil	0.20	5.20E-07	1.33	0.35	0.050	0.0100
grass, short, on wet soil	0.20	5.20E-07	1.33	0.55	100.000	0.0100
grass, long, on dry soil	0.20	5.20E-07	1.33	0.35	0.070	0.0200
grass, long, on wet soil	0.20	5.20E-07	1.33	0.55	100.000	0.0200
cropland	0.20	5.20E-07	1.33	0.40	0.060	0.0400
cropland, irrigated	0.20	5.20E-07	1.33	0.65	100.000	0.0400
cropland, on sandy soil	0.20	5.20E-07	1.33	0.35	0.040	0.0400
heath	0.15	5.70E-07	1.05	0.15	0.423	0.0500
heath, on sandy soil	0.15	5.70E-07	1.05	0.15	0.100	0.0500
bushes, short, on dry soil	0.20	5.20E-07	1.33	0.15	0.060	0.1000
bushes, short	0.20	5.20E-07	1.33	0.35	0.090	0.1000
forest, deciduous	0.17	8.00E-07	2.16	0.60	0.120	1.0000
forest, coniferous	0.10	8.00E-07	2.16	0.50	0.160	1.0000
forest, coniferous, on wet soil	0.10	8.00E-07	2.16	0.70	100.000	1.0000
forest, mixed	0.15	8.00E-07	2.16	0.45	0.120	1.0000
forest, mixed, on dry soil	0.15	8.00E-07	2.16	0.50	0.050	1.0000
forest, mixed, on wet soil	0.15	8.00E-07	2.16	0.50	100.000	1.0000
forest and bushes	0.20	6.50E-07	1.75	0.20	0.100	0.2500
buildings, low	0.18	14.0E-07	2.61	0.50	0.002	0.6000
buildings, high	0.18	23.0E-07	3.44	0.50	0.002	1.2000
mixed surface cover	0.20	5.20E-07	1.33	0.20	0.100	0.10000

that the target variable of the SDD is the average strong UHI pattern instead of the average UHI pattern. The "relevant days", which should be simulated for each WP are those days with ΔT_{u-r} closest to $(\Delta T_{u-r})_{\mathrm{Thres}}$ and the day with the maximum ΔT_{u-r} ($(\Delta T_{u-r})_{\max}$). Thus 14 days are selected. Since the UHI is not an instantaneous event developing in a dynamical model right after initialization, for each relevant day a 3 day period is simulated. The longer initialization is needed to ensure realistic heat storage in the urban fabric, which is one of the drivers for UHIs.

For the downscaling from the ERA40 reanalysis of ~115 km horizontal resolution to 1 km, at least a 4 step nesting would be needed (e.g. 48 km, 12 km, 4 km, and 1 km) when using a refinement factor of 4. The numerical model METRAS is not designed for horizontal resolutions larger than about 20 km (Schlünzen et al., 2012a). Therefore, an intermediate model would be needed to simulate the outer domain, as e.g. done by Huebener and Kerschgens (2007a,b). To avoid this step, high resolution analysis fields from the ECMWF are used as forcing. The ECMWF data and the forcing technique are explained in detail in Section 4. The analysis data are available at a resolution of ~ 25 km starting in 2006, leaving the period 2006–2010 to determine the relevant days. During that period, neither observations of the UHI nor ERA40 based WP data are available. To extend the ERA40 based WP time series, the WPs are determined for the ERA-Interim (ERA-INT) dataset (Dee et al., 2011). ERA-INT is an improved and frequently updated atmospheric reanalysis dataset starting in 1979. An investigation of the WP time series of both datasets for the overlapping time period 1979–2001 showed that they are identical for more than 99 % of the days. The values for ΔT_{u-r} are calculated with the statistical model (Eq. (2.1)). The selected relevant days and their corresponding simulation names are listed in Table 1. For WP7, both $(\Delta T_{u-r})_{\mathrm{Thres}}$ and $(\Delta T_{u-r})_{\max}$ are equal, resulting in only one mesoscale model simulation required for this WP.

In order to calculate the average strong UHI, the simulation results obtained with METRAS at 1 km horizontal resolution (METRAS-1 km) need to be recombined statistically. For this, the UHI pattern for each relevant-day is calculated from METRAS-1 km output by subtracting rural temperature values from the temperature field (Section 5.1). The resulting UHI patterns contribute to the average strong UHI pattern with a specific weight. The weight of each simulation is based on the frequency of occurrence of the corresponding WP and the statistical modelled UHI (ΔT_{u-r}, Eq. (2.1)). The UHI pattern of a given day with $\Delta T_{u-r} \geq 3\,\mathrm{K}$ is a linear combination of the two UHI simulated patterns UHI($(\Delta T_{u-r})_{\max}$) and UHI($(\Delta T_{u-r})_{\mathrm{Thres}}$), which are obtained for each WP. Consequently, the weights for the kth WP also depends on the number of strong UHI days N_{strong} for the corresponding WP (Eq. (2.2)) and the difference between the maximum UHI $(\Delta T_{u-r})_{\max}$ and the threshold UHI $(\Delta T_{u-r})_{\mathrm{Thres}}$, which is denoted as R_{strong} (Eq. (2.3)).

$$N_{\mathrm{strong}}(k) = \sum_{\Delta T_{u-r} \in WP(k)} \begin{cases} 1 & \text{if } \Delta T_{u-r} \geq 3\,\mathrm{K} \\ 0 & \text{if } \Delta T_{u-r} < 3\,\mathrm{K} \end{cases} \tag{2.2}$$

$$R_{\mathrm{strong}}(k) = (\Delta T_{u-r})_{\max}(k) - (\Delta T_{u-r})_{\mathrm{Thres}}(k) \tag{2.3}$$

The absolute differences between $\Delta T_{u-r} \geq 3\,\mathrm{K}$ and $(\Delta T_{u-r})_{\max}$ as well as between $\Delta T_{u-r} \geq 3\,\mathrm{K}$ and $(\Delta T_{u-r})_{\mathrm{Thres}}$ are normalized by R_{strong} then summed up for each WP. These sums are then divided by N_{strong} to yield the averaged non-dimensional differences $Diff_{\max}$ (Eq. (2.4)) and $Diff_{\mathrm{Thres}}$ (Eq. (2.5)) assuming $N_{\mathrm{strong}}(k)$ to be greater than 0, which is true in the present study.

$$Diff_{\max}(k) = \left(\sum_{\Delta T_{u-r} \geq 3\,\mathrm{K} \in WP(k)} \frac{(\Delta T_{u-r} - (\Delta T_{u-r})_{\mathrm{Thres}}(k))}{R_{\mathrm{strong}}(k)} \right) \cdot (N_{\mathrm{strong}}(k))^{-1} \tag{2.4}$$

$$Diff_{\mathrm{Thres}}(k) = \left(\sum_{\Delta T_{u-r} \geq 3\,\mathrm{K} \in WP(k)} \frac{((\Delta T_{u-r})_{\max}(k) - \Delta T_{u-r})}{R_{\mathrm{strong}}(k)} \right) \cdot (N_{\mathrm{strong}}(k))^{-1} \tag{2.5}$$

These averaged differences represent the weights of both simulations within each WP. The final weights $W_{\max}$ and W_{Thres} are calculated by multiplying Eq. (2.4) and Eq. (2.5) with the corresponding relative frequency of N_{strong}.

$$W_{\max}(k) = Diff_{\max}(k) \cdot \frac{N_{\mathrm{strong}}(k)}{\sum_{i=1}^{K} N_{\mathrm{strong}}(i)} \tag{2.6}$$

$$W_{\mathrm{Thres}}(k) = Diff_{\mathrm{Thres}}(k) \cdot \frac{N_{\mathrm{strong}}(k)}{\sum_{i=1}^{K} N_{\mathrm{strong}}(i)} \tag{2.7}$$

Days with $\Delta T_{u-r} > (\Delta T_{u-r})_{\max}$ are treated as days with a $\Delta T_{u-r} = (\Delta T_{u-r})_{\max}$ since an extrapolation of the pattern is not possible. This case can occur because $(\Delta T_{u-r})_{\max}$ is only determined in the period 2006–2010 and because large values of $(\Delta T_{u-r})_{\max}$ could occur in the future climate projections. Thus, UHI changes from current to future climate might be slightly underestimated.

The statistically recombined UHI pattern is computed by multiplying $W_{\max}$ and W_{Thres} with the corresponding simulated UHI patterns and summing up the resulting patterns. For the current climate (1971–2000), the weights are calculated from the WPs based on the ERA40 data and the statistically modelled UHI values computed with DWD observations from Hamburg-Fuhlsbüttel. To determine changes in the UHI pattern due to climate change, the weights are calculated for the different RCM results, described in Section 3. In this study, changes between the current climate period (1971–2000) and two future climate periods (2036–2065 and 2070–2099) are investigated. Using the introduced SDD method, the average strong UHI pattern can change due to frequency changes of the WPs as well as due to changes in the distribution of statistically modelled strong UHI values within the corresponding WP.

3 Regional climate model data

As used by Hoffmann et al. (2012) and Hoffmann and Schlünzen (2013), data from the regional climate simulations conducted with CLM (Hollweg et al., 2008) and REMO (Jacob et al., 2008) are used as input for the downscaling. Both RCMs are driven with the SRES A1B projections from ECHAM5-MPIOM (Roeckner et al., 2003; Jungclaus et al., 2006). The REMO simulations have been conducted by applying a two-step nesting. Since the domain with the finest grid is smaller than the domain used for the WPC, the WPs are determined from the coarser simulations (~50 km). The variables for the statistical model are determined from the high-resolution simulations (~ 10 km).

Schoetter et al. (2012) evaluated the CLM and REMO results for the metropolitan area of Hamburg. For both RCMs, considerable biases in some of the variables used for the statistical model of the UHI have been found for the present climate. These biases also lead to biases in the statistically modelled UHI (Hoffmann et al., 2012). Therefore, the RCM data are bias-corrected with ERA-40 data following Schoetter et al. (2012), by applying a quantile-mapping method similar to Piani et al. (2010). A problem appearing when using the bias-correction for the SDD method is that the local variables, and therefore the statistically modelled UHI, might not be consistent with the WPs after the bias correction. In future studies, it should be tested if the bias-correction could be done for each WP separately. Hoffmann and Schlünzen (2013) also showed that there are biases in the frequency of the WPs in the RCM results. A bias correction method for the daily atmospheric patterns is, however, not yet available. Only the WP frequencies could be bias-corrected, as suggested by Demuzere et al. (2009). This is not applicable for the SDD

method presented in this study, because in the calculation of the weights (Eq. (2.6) and Eq. (2.7)), the WPs and the statistically modelled UHI depend on each other. Hence, for the present study only the biases in the surface variables, which go into the statistical model, are corrected as described in Schoetter et al. (2012).

4 Dynamical simulations

4.1 Mesoscale model

The mesoscale transport and fluid model METRAS (Schlünzen, 1990; Lüpkes and Schlünzen, 1996) is a three-dimensional non-hydrostatic mesoscale numerical atmospheric model. It has been previously applied to Germany (Schlünzen, 1992; Renner and Münzenberg, 2003; Schlünzen and Katzfey, 2003; Schüler and Schlünzen, 2006; Schlünzen and Meyer, 2007; Bohnenstengel, 2011, Buschbom et al., 2012), Spain (Augustin et al., 2008), China (Wu and Schlünzen, 1992; Sheng et al., 2000), coastal areas (Niemeier and Schlünzen, 1993; Boettcher et al., 2015), the Arctic (Dierer and Schlünzen, 2005; Hebbinghaus et al., 2007; Lüpkes et al., 2008; Ries et al., 2010) and the urban climate of London (Thompson, 2008; Grawe et al., 2012) with horizontal resolutions ranging from 1 km to 18 km. A detailed description of METRAS is given in Schlünzen et al. (2012a). The dynamic equations solved in METRAS are based on the anelastic and Boussinesq approximated primitive equations, resulting in prognostic equations for the three wind-components u, v and w, potential temperature and specific humidity. Microphysical cloud processes are parameterized with a Kessler liquid-only scheme (Kessler, 1969), using prognostic equations for cloud water content and rain water content. The radiation parameterization is dependent on the existence of liquid water in the model domain. In cloud free situations, the longwave and shortwave radiation balance is computed only at the surface. In that case, a constant cooling rate of 2 K/day at daytime and 3 K/day at nighttime is assumed in the atmosphere. With clouds in the model domain, the radiation fluxes at the surface as well as in the atmosphere are determined with a two-stream approximation scheme. The equations are numerically solved in flux form on an Arakawa-C-grid (Mesinger and Arakawa, 1976), where the wind components (u, v, and w) are shifted by half a grid point compared to the grid points of scalar quantities.

The surface layer similarity theory is employed for the calculation of sub-grid scale turbulent fluxes in the surface layer ($z \leq 10$ m). The flux averaging method is applied for different fractions of surface cover within a grid cell. It is implemented using the blending height concept (Claussen, 1991; von Salzen, 1996). The different surface cover classes are described in Section 4.2. For water surfaces, the roughness length is a function of wind speed and in particular of the friction velocity (Brutsaert, 1972).

The vertical turbulent fluxes above the surface in the stable and neutrally stratified boundary layer are parameterized using a mixing length scheme based on Herbert and Kramm (1985). For unstable stratification, the non-local countergradient scheme is used (Lüpkes and Schlünzen, 1996) allowing mixing of momentum, heat and moisture counter the local gradient.

To calculate the surface temperatures T_S, the force-restore method by Deardorff (1978) is applied. The equation for the surface temperature tendency can be written as:

$$\frac{\partial T_S}{\partial t} = \frac{2\sqrt{\pi}k_s}{\nu_s h_\theta}\Big\{B_s - B_l + c_p\rho_0 u_*\theta_* + l_{21}\rho_0 u_* q_* - \sqrt{\pi}\nu_s\frac{\overline{T_S} - \overline{T_S}(-h_\theta)}{h_\theta}\Big\} \quad (4.1)$$

The first two terms on the right hand side correspond to the shortwave and longwave radiation budget at the surface.

Term three in Eq. (4.1) accounts for the surface temperature change due to the sensible heat flux, which depends on the heat capacity c_p, the density of the air ρ_0 and the turbulent heat flux $u_*\theta_*$, where u_* and θ_* denote the friction velocity and the scaling value of temperature, respectively.

The fourth term corresponds to the temperature change due to the latent heat flux, which depends on the enthalpy of vaporization l_{21} and the turbulent humidity flux, where q_* denotes the scaling value of specific humidity. The last term on the right hand side reflects the ground heat flux, i.e. heat release or heat storage depending on the soil and surface cover characteristics, the depth of the daily temperature wave h_θ and thermal conductivity of the soil ν_S. Since each simulation conducted in this study is done for a 3 day period the temperature at the depth of the daily temperature wave $\overline{T_S}(-h_\theta)$ is kept constant at its initial value. For the specific humidity at the surface, a simple budget equation is applied (Deardorff, 1978).

In the METRAS version applied, no additional urban canopy parameterization is implemented as done by Thompson (2008). Therefore, the influence of buildings on the radiation within street canyons (e.g. shading and radiative trapping) as well as on the flow field within the canopy layer is not considered. Furthermore, the anthropogenic heat release is neglected. Hence, only urban effects due to the different surface characteristics such as heat storage, water availability, evaporation characteristics and roughness are simulated. A detailed description of the surface characteristics as used in the present study is given in the next Section.

4.2 Model domain and land use

The dynamical simulations are conducted by forcing METRAS at 4 km horizontal resolution (METRAS-4 km) with ECMWF analysis data and using these results to force a simulation with 1 km horizontal resolution (METRAS-1 km). The boundaries of both domains

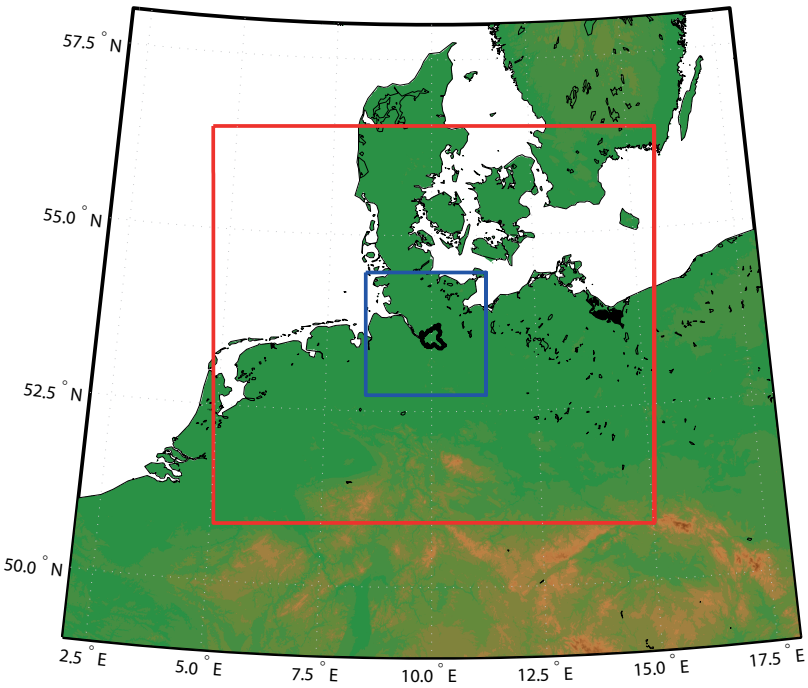

Figure 2: Map indicating the boundaries of the METRAS-4 km domain (red) and METRAS-1 km domain (blue).

are shown in Fig. 2. The outer domain has a dimension of 175×156 grid cells (700 km×624 km) covering northern Germany, and parts of Denmark, the Netherlands, Sweden and Poland. The dimension of the inner domain is 194 × 191grids cells (194 km × 191 km) and it covers the metropolitan area of Hamburg including parts of the North Sea and Baltic Sea. The vertical grid of both domains follows the terrain and consists of 34 vertical levels. The lowest model level is at 10 m above ground. The vertical grid spacing is 20 m up to a height of 90 m above ground. Above that level, the grid spacing increases with a constant stretching factor of 1.15. The top of both domains is at 12511 m.

To construct surface cover data (lower boundary condition for METRAS), land-use data from different sources are used, ranging from the "European Commission programme to Coordinate Information on the Environment" (CORINE) dataset from 2006, a digital basic map (ATKIS), information on building outlines to a detailed biotope dataset for the state of Hamburg. For METRAS-4 km, the land-use data are aggregated into 10 land-use classes including one urban land-use class. For the METRAS-1 km simulations, the land-use data are aggregated to 36 surface cover classes. Flagg et al. (2011) comprehensively investigated urban land-use types, such as "block perimeter development", and determined the fraction of buildings, sealed surfaces (asphalt, concrete, brick/pavers), as well as urban vegetation (e.g. street trees, courtyard vegetation and so on). These fractions have been used to assign the land-use data to the appropriate surface cover classes. Buildings are divided into high buildings and low buildings. The physical parameters attributed to the surface cover classes are given in Table 1. Details on the attribution of the parameter values are given in Schlünzen et al. (2012b). Fig. 3 shows the fraction of buildings and adjacent surfaces, which include the surface cover classes "high buildings", "low buildings", "asphalt", "concrete", "brick/pavers" and "steel". Here, the sealing gradient of Hamburg (highest values near the centre of the city and in industrial and harbour areas, lower values in the outskirts of the city) is well visible. In addition, it shows that even in the centre of Hamburg, the sealed fraction is well below 1. This is due to the presence of water (e.g. canals), street trees and courtyard vegetation even in the centre of the city.

4.3 Forcing

To simulate the selected meteorological situations, METRAS needs to be forced with interpolated observational data or model results of coarser resolution. Analysis data provided by the ECMWF (ECMWF, 2009; 2010) are suitable for this purpose (Ries et al., 2010). ECMWF-analyses are available every six hours (00 UTC, 06 UTC, 12 UTC, and 18 UTC). The horizontal resolution varies according to the resolution of the actual ECMWF forecast model. From 2006 to January 2010, the grid resolution is T799L91, which corresponds to a horizontal resolution of ~ 25 km and 91 vertical levels. The model levels use terrain following pressure coordinates. The resolution increased to T1279L91 (~ 16 km) starting end of January 2010. Hence, simulations for 2010 have finer forcing data than the rest of the simulations. Forced variables are potential temperature, horizontal wind components and specific humidity. Liquid and ice water content are added to the specific

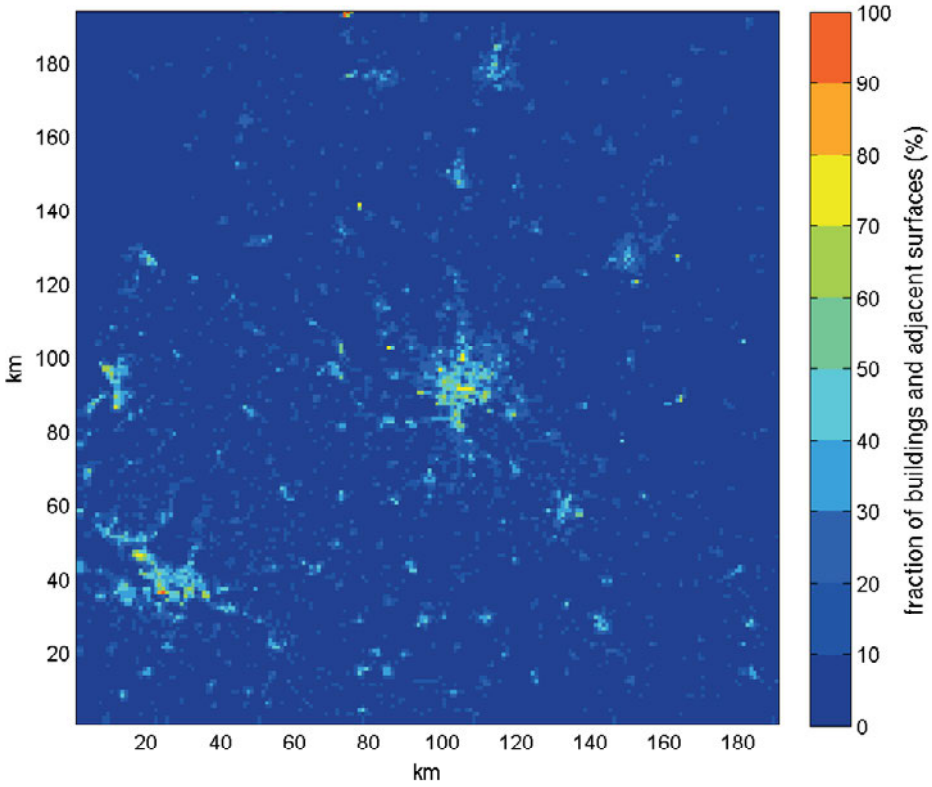

Figure 3: Fraction of buildings and adjacent sealed surfaces in a $1 \times 1\,\mathrm{km}^2$ grid cell as a sum of the surface cover classes: high buildings, low buildings, asphalt, concrete, brick/pavers and steel from METRAS-1 km data.

humidity. This allows METRAS to develop clouds consistent with its model physics. A linear interpolation of the forcing data to the METRAS grid is made.

For water temperatures, the optimum interpolation sea surface temperatures (OISST) analysis dataset (Reynolds et al., 2002), provided by NOAA, are used. It consists of weekly averaged SST data with a spatial resolution of 1° (~110 km). In analogy to the atmospheric variables, the SSTs are interpolated horizontally to the corresponding METRAS grid points. The temperatures of rivers and lakes are estimated using interpolated SSTs through the continent (Bungert, 2008) and height corrected using the standard atmosphere lapse-rate of $-0.0065\ \mathrm{Km}^{-1}$. The temperatures at the depth of the daily temperature wave, which are required by METRAS, are set to be equal to the water temperatures, because no reliable soil temperatures have been available for this study.

Since METRAS is initialized with a 1D profile that is homogenously distributed over the whole domain and height corrected within a diastrophy phase using a dynamical initialization, an averaged profile is determined from forcing data. After the diastrophy phase information from the coarser data is forced onto the finer grid solution using the nudging technique. For this, a so-called forcing term is added to the prognostic equations for potential temperature, specific humidity, u- and v-velocity (Eq. (4.2)).

$$\Psi_f = \Psi_m + \delta(\Psi_l - \Psi_m) \tag{4.2}$$

with

$$\delta = \nu \Delta t \tag{4.3}$$

Here Ψ_m is the original value of a prognostic variable, Ψ_l is the value of the variable in the forcing data, Ψ_f is the resulting value after the forcing, and δ is the weighting factor which depends on the time step Δt and the nudging coefficient ν. For the first hour after the initialization, $\nu = \nu_0$ (homogenous forcing) is set to $0.001\ \mathrm{s}^{-1}$. This corresponds to a characteristic time of about 17 minutes, implying that the resulting values are equal to the forcing value after 17 minutes. The homogenous forcing lasts for 1 hour of integration time. Thereafter, the forcing decreases within the domain and the nudging coefficient becomes:

$$\nu(i) = \nu_0(i - \tanh(\frac{a_f}{N_f - 3} i)) \tag{4.4}$$

In this study, a_f and N_f are set 0.4 and 4 respectively. The nudging coefficient depends on the grid point distance to the lateral and upper boundaries. The decrease in forcing towards the inner of the model domain makes sure that the METRAS model can reproduce small-scale meteorological features, but still accounts for large-scale changes due to the relatively strong forcing at the boundaries. Since the forcing data are not available for every model time step, they are linearly interpolated in time.

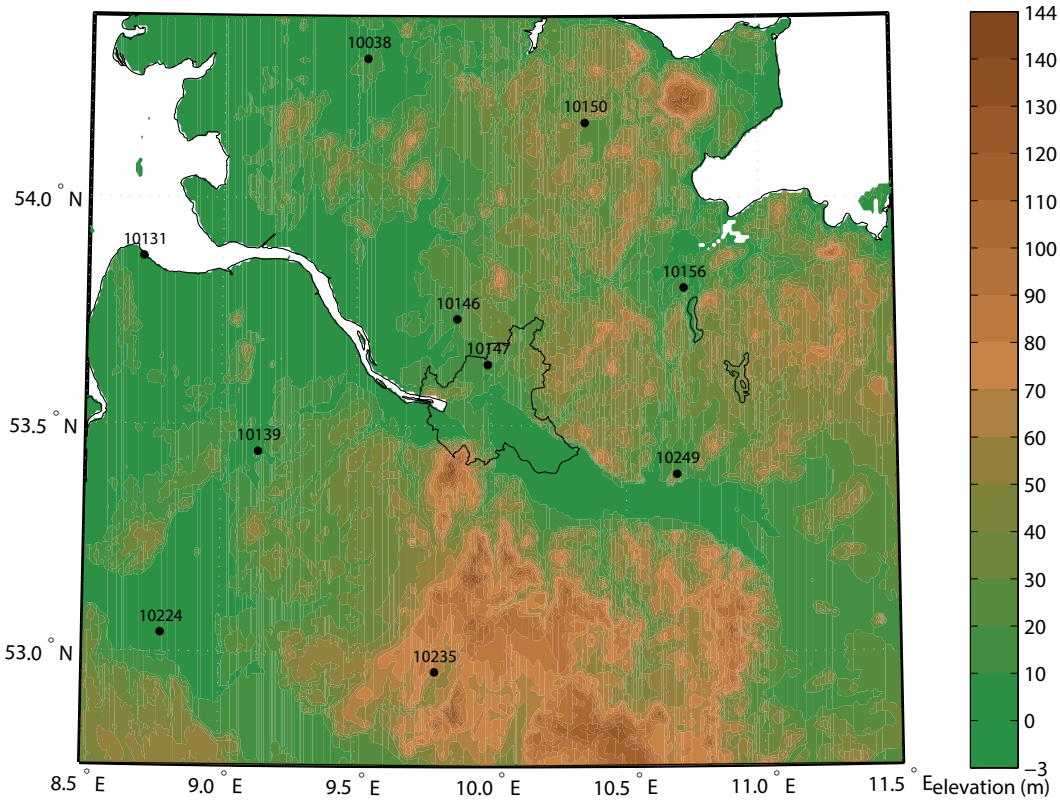

Figure 4: Location and WMO number of the SYNOP stations used for the evaluation of the dynamical simulations.

4.4 Evaluation of dynamical runs

An advantage of the downscaling method introduced in the present study is that model results can be evaluated against observed data. Most of the dynamical and statistical-dynamical downscaling techniques do not allow this, because they are forced with climate projections and not with analysis or reanalysis data. In this study, the evaluation focuses on hourly values of near surface data.

4.4.1 Observational data

In this study, data measured at SYNOP stations operated by DWD are used for model evaluation. SYNOP stations provide hourly values of 2 m temperature, 2 m dew point, sea level pressure, cloud cover, 10 m wind speed and direction. In the framework of this study, only stations with measurements available for at least 95 % of the time for the period between 2006 and 2010 are used. This assures the comparability of the evaluation results between the different simulations. In total, 10 stations match that criterion (Figure 4).

4.4.2 Evaluation method

There are several ways to evaluate model results. A well-established approach is the comparison of model estimates with near-surface observations (Cox et al., 1998; Schlünzen and Katzfey, 2003; Ries and Schlünzen, 2009). The model results are horizontally interpolated to the location of the corresponding station by using bi-linear interpolation. The simulated meteorological variables at the first model level in 10 m above ground are used in the present evaluation, because the corresponding gird-averaged values in 2 m above ground cannot be reliably determined due to the use of the flux aggregation approach. The focus of the evaluation presented in this section is on the variables temperature, relative humidity, wind speed, and wind direction. Temperature is chosen because the target parameter of the statistical-dynamical downscaling, the UHI is a horizontal temperature difference. Relative humidity and wind speed are chosen, because Hoffmann et al. (2012) demonstrated that both parameters are important for the strength of Hamburg's UHI. Usually, other parameters related to atmospheric moisture content, such as water vapour pressure or dew point are evaluated, because the error in the simulated relative humidity is not only due to shortcomings in the simulation of the hydrological processes. However, these parameters are only weakly correlated to the UHI (Hoffmann et al., 2012). Therefore, it is more important to accurately simulate the relative humidity. The wind direction is important for advection of the UHI. Statistical measures are used to quantitatively evaluate the model performance. Following the model evaluation guideline of COST728 (Schlünzen and Sokhi, 2008), the differences in the means of a variable (*BIAS*; Eq. (4.5)) and the hit-rate (*HITR*; Eq. (4.6)) are calculated.

$$BIAS = \bar{M} - \bar{O} \tag{4.5}$$

$$HITR = \frac{1}{N}\sum_{i=1}^{N} n_i \text{with} n_i \begin{cases} 1 & \text{if } |M_i - O_i| \leq D \\ 0 & \text{else} \end{cases} \quad (4.6)$$

Here, O_i and M_i denote the observation and the corresponding model result, $\bar{O}$ and $\bar{M}$ denote the corresponding means, and N is the sample size. The *BIAS* indicates whether a variable is generally overestimated or underestimated and if so, to what extent. The *HITR* indicates how often the model results lie within the demanded forecast accuracy, a given predefined uncertainty range to the observed value that also accounts for the observation uncertainty. The optimal value for *HITR* is 1, which indicates that all model results lie within the uncertainty D of the observation and the minimum value is 0, which indicates that none of the model results is within the uncertainty of the observations. The values for D for temperature (2 K), wind speed (1 ms^{-1} for $ff < 10\,ms^{-1}$ and 2.5 ms^{-1} for $ff > 10\,ms^{-1}$), and wind direction (30°) are taken from Cox et al. (1998). For temperature and wind speed, they are close to the findings of Lengfeld and Ament (2012) and Lengfeld (2012), who, using a sensor network, investigated the representativeness of 2 m temperature and wind speed over heterogeneous terrain. For instance, they found that temperature differences between stations (computed every minute) can be 3 K or higher on a distance of about 2 km in a heterogeneous terrain. For relative humidity, the value of D is set to 5 %.

The measures for wind direction are calculated differently to the other variables. The mean wind direction is computed by calculating the u- and v-component of the velocity vector using the wind speed. Thereafter, u and v are averaged component-wise. The average wind direction is the direction of the resulting vector. The wind direction cannot be measured accurately for low wind speeds. Hence, only wind data for measured wind speeds > 1 ms^{-1} are used for the evaluation. To visualize the results, the measures calculated for every station are averaged over all stations.

In addition to the strict comparison of observations and model results, a so-called persistence forecast is computed as a benchmark for the skill of the model result. For the persistence forecast, the observations of the initial day are used as a forecast for the following days. During anticyclonic conditions with weak large-scale forcing, the model could perform worse than the persistence forecast. In such meteorological situations, the dependency of the model results on the initial conditions and the boundary conditions at the surface, such as the water and soil temperatures or surface cover data, is very large. For instance, surface temperature gradients could lead to development of a local circulation not observed in reality and thus being an artefact of the initially selected soil and water temperatures.

4.4.3 Evaluation results

The statistical measures are calculated for both METRAS-4 km and the METRAS-1 km simulations based on 10 stations. The results for day 2 of the simulations are displayed in Fig. 5. The largest differences between both resolutions are found for the temperature and the wind direction. The results for both resolutions are only marginally different for relative humidity and wind speed. On average, METRAS-1 km performs slightly better for the wind speed (Fig. 5e,f). The simulation of the wind direction improves in the higher resolution model experiment as well. The *HITR* improves from 0.40 to 0.44 (Fig. 5g) and the averaged *BIAS* from -30° to -10°. However, the averaged absolute *BIAS* is only slightly reduced. For relative humidity, METRAS-4 km shows almost no difference in performance regarding the average *HITR* (Fig. 5c). The averaged *BIAS* is only 1 % for METRAS-4 km, while METRAS-1 km overestimates the relative humidity by almost 7 % (Fig. 5d). Overall, 4 simulations with METRAS-1 km show a *BIAS* of more than 10 %. The higher relative humidity might be a reason for the lower temperatures (Fig. 5b) and lower *HITR* for temperature (Fig. 5a) compared to METRAS-4 km. The *HITR* of METRAS-1 km is reduced to the level of the persistence forecast. For the rest of the variables both METRAS-1 km and METRAS-4 km perform better than the persistence forecast when comparing *HITR*. The averaged absolute *BIAS* of the METRAS simulations is lower for all variables.

5 Statistically-dynamically downscaled average strong summer urban heat island

5.1 Current climate

The UHI needs to be calculated for each simulation separately to statistically recombine the results of the dynamical simulations. Generally, there are two methods to determine the UHI from one simulation. The first method is to conduct two simulations, one with the actual surface cover and one without the urban surfaces, and subtract both simulation results from each other (e.g. Hjemfelt, 1982; Hafner and Kidder, 1999; Zhou and Shepherd, 2009; Grawe et al., 2012). This method would double the computational cost and additional problems arise, such as the composition of the non-urban surface cover. Hence, it is not applicable for the present study. The second method involves subtracting the temperature at rural grid points from the whole temperature field (e.g. Flagg, 2010). Since this method does not require additional simulations and is straight forward to compute, it is used in context of this study. However, the choice of the rural grid points can strongly impact the calculated UHI (e.g. artificially strong UHI due to the presence of cold pools at the rural grid points). A comparison of the magnitude of simulated and observed UHI is therefore challenging.

The temperature values in 10 m above ground from the grid points closest to the two DWD stations Grambek and Ahrensburg are averaged to obtain a rural temperature value. To compare the numerically simulated

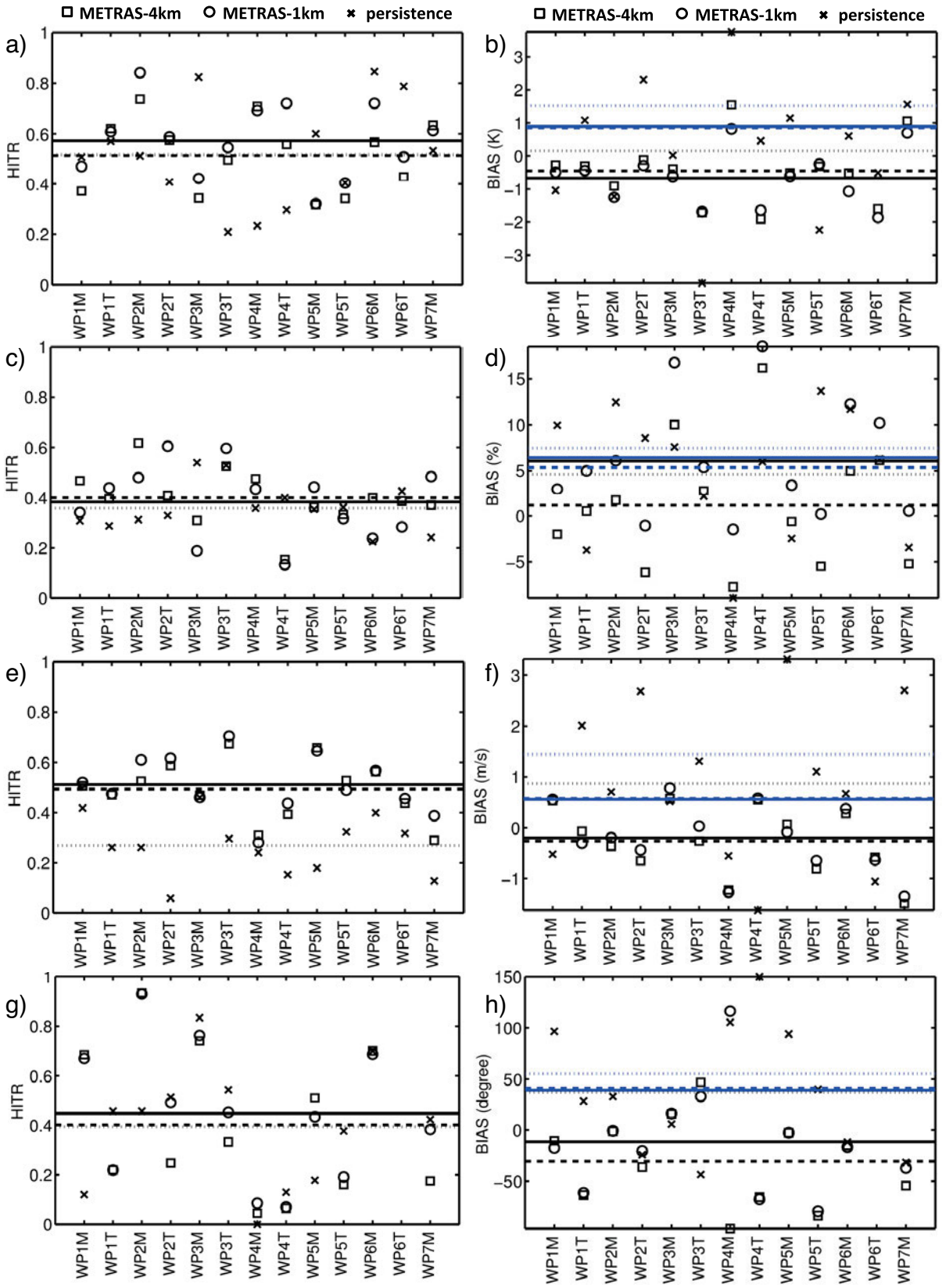

Figure 5: HITR and BIAS of (a,b) temperature, (c,d) relative humidity, (e,f) wind speed and (g,h) wind direction for METRAS simulations of model day 2. Solid lines indicate the mean (black) of HITR and BIAS, and mean absolute BIAS (blue) of METRAS-1 km simulations. Dashed lines indicate the mean (black) of HITR and BIAS and mean absolute BIAS (blue) of METRAS-4 km simulations. Dotted lines indicate the mean (black) and mean absolute BIAS (blue) of the persistence forecast.

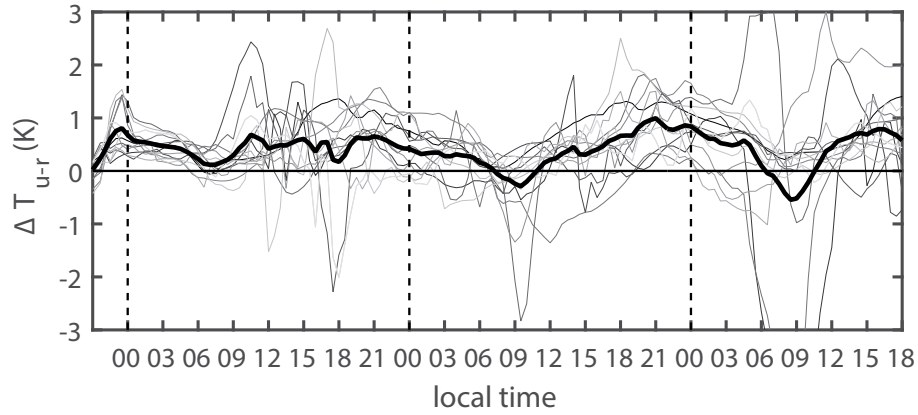

Figure 6: Simulated time series of the urban-rural temperature difference ΔT_{u-r} from all 13 simulations (Table 1) conducted with METRAS-1 km. Black solid line indicates the unweighted average of all simulations.

Table 2: List of relevant days and their corresponding statistically modelled UHI values ΔT_{u-r}. The number within the simulation names denotes the WP number, while the ending denotes maximum UHI day (M) or the day with an UHI closest to the threshold UHI (T).

Simulation name	Date	ΔT_{u-r} (K)
WP1M	17-Jun-2007	4.6
WP1T	22-Jun-2009	3.0
WP2M	09-Jul-2007	3.3
WP2T	19-Aug-2007	3.0
WP3M	05-Jul-2006	5.7
WP3T	01-Jul-2009	3.0
WP4M	01-Aug-2009	4.0
WP4T	18-Jul-2009	3.0
WP5M	17-Aug-2008	4.1
WP5T	18-Jun-2008	3.0
WP6M	11-Jun-2007	5.2
WP6T	17-Jul-2009	3.1
WP7M	06-Jun-2009	3.2

UHI values with the statistically modelled UHI (Section 2) and to investigate the temporal variability of the UHI intensity, the temperature in 10 m above ground close to the DWD station Hamburg-St. Pauli is used to represent the urban temperature as in Hoffmann et al. (2012). The time series of the simulated urban-rural temperature differences ΔT_{u-r} obtained from the METRAS-1 km simulations is shown in Fig. 6. The urban-rural temperature differences ΔT_{u-r} are quite different for different WPs. All differences are smaller than the corresponding statistically modelled values as shown in Table 2. Possible reasons for this inconsistency are given in Section 6.

Nevertheless, the ΔT_{u-r} time series shows a typical diurnal cycle of the temperature differences (Oke, 1987) on day 2 and day 3. Neglecting the frequency of occurrence, the average of all simulations shows positive differences from noon to the early morning (around sunrise) with a maximum between 8 p.m. and 12 a.m. (midnight) local standard time (LST). Negative values of the UHI are simulated between 7 a.m. and 12 p.m. (noon) LST. After sunrise, rural areas heat up at higher rates than urban areas. This so-called urban cool island (UCI) is mainly due to the high thermal conductivity and diffusivity of urban surfaces. More heat is taken up by the sealed surfaces in urban areas compared to the surfaces in rural areas. This leads to a reduction of the heating rate of the air during the morning hours. The UCI effect has also been found for Hamburg by Schlünzen et al. (2010) by analysing the DWD station data. They showed that on average, the daily maximum temperature within the city is slightly lower compared to Grambek, especially in summer. Later during the day, this effect becomes less important and disappears after sunset.

Investigation of the individual time series reveals substantial temporal variability of UHI. The large positive and negative values throughout the four simulation days are mainly resulting from clouds (i.e. increase in downward long-wave radiation). Due to their random nature, the presence of clouds renders the calculation of the UHI challenging, especially due to the low number of grid points that have been used to calculate the UHI. Using data from only one model output time step to compare simulations could result in large differences not due to urban effects, but due to the presence of small clouds. Therefore, the nocturnal UHI intensity is defined as the average temperature difference between 8 p.m. and 12 a.m. LST, when the averaged temperature difference is largest (thick line in Fig. 6). The simulated $(\Delta T_{u-r})_{\max}$ is lower than $(\Delta T_{u-r})_{\text{Thres}}$ for WP2 and WP5 (not shown). This could be due to the accuracy of the statistical model, which was used to identify the days that are simulated. It explains only 50 % of the UHI variance and has a RMSE of 1.2 K (Section 2). This difference is larger than the difference between $(\Delta T_{u-r})_{\max}$ and $(\Delta T_{u-r})_{\text{Thres}}$ in the corresponding WPs. However, the effect on the statistically recombined average strong UHI pattern is small, because the sum of the weights of WP2 and WP5 is only 0.06.

To compute the average strong UHI pattern (Section 2), the frequency of the ERA40 WPs and the statistically modelled UHI based on the observations from Hamburg-Fuhlsbüttel in the period 1971–2000 are used to calculate the weights for the different simulations ac-

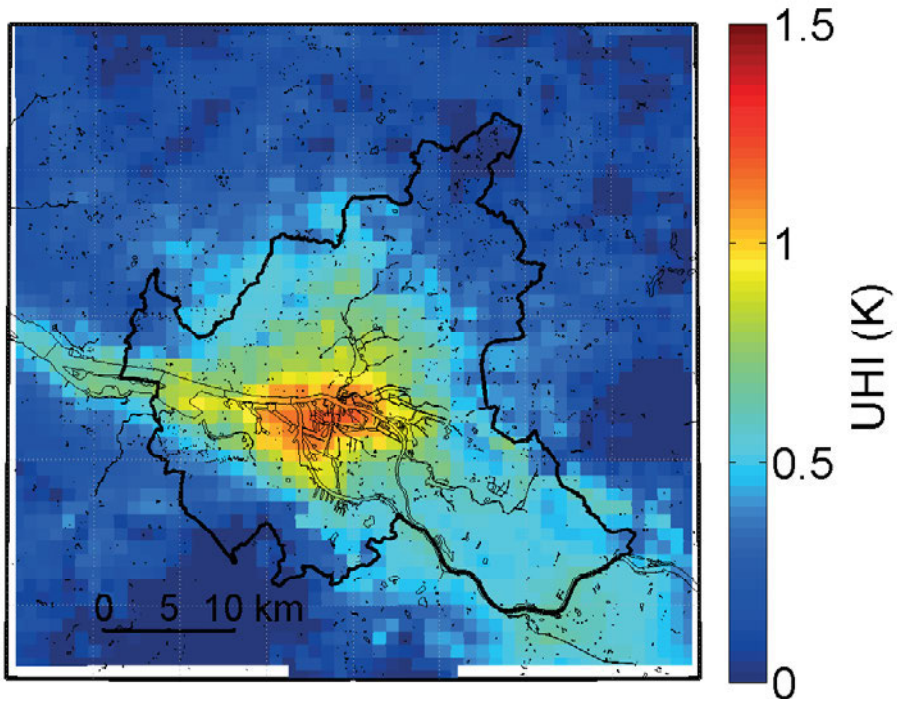

Figure 7: Statistically recombined average strong UHI (8 p.m. to 12 a.m. LST) pattern using data for the period 1971–2000 for summer METRAS-1 km simulations.

cording to Eq. (2.6) and Eq. (2.7). Thereafter, the individual UHI patterns are multiplied with their corresponding weights (Section 2). For 1971–2000, on average 24.9 strong UHI days (statistically modelled UHI ≥ 3 K) occur in the summer season. The average strong UHI pattern calculated from METRAS-1 km results is displayed in Fig. 7. The maximum of the UHI intensity (up to 1.2 K) is found in the harbour and in downtown Hamburg. This is due to the large fraction of sealed surfaces in this area. The river Elbe also contributes to the high UHI values in this area due to weak nocturnal cooling of the air over water bodies, which have a constant temperature throughout each simulation. This effect is responsible for the increased nocturnal temperatures in the western part of the city, i.e. where the river is relatively wide. A detailed examination of the pattern reveals that structures such as the two airports within Hamburg namely Fuhlsbüttel (north of the Alster lake) and Finkenwerder (western part of Hamburg), can be identified. Both areas show higher temperatures than their surroundings. Relatively high temperatures are simulated in the rural southeast of Hamburg. This might again be due to the Elbe river, which flows through that area. In addition, the elevation of the area is low compared to the rural reference grid points. After applying a height correction to the results the UHI intensity is close to 0 K in this area except for the grid points along the river (Fig. 5.14 in Hoffmann, 2012).

5.2 Evaluation of the UHI pattern

Only few meteorological observations are available to evaluate Hamburg's UHI pattern. However, the observed temperature differences between the rural station Grambek and six stations in and around Hamburg are correlated with the simulated UHI pattern as it was also done by Bechtel and Schmidt (2011) for the temperature proxy data. For the comparison, as derived by Schlünzen et al. (2010), the annually averaged UHI and the summer-averaged UHI are used. Additionally, the UHI pattern constructed by Bechtel and Schmidt (2011), which used floristic mapping data, is compared with the numerically simulated UHI patterns. The so-called Ellenberg indicator values for temperature (EIT) are used as proxies for the temperature distribution within Hamburg. As described by Bechtel and Schmidt (2011), a linear regression with the UHI values given by Schlünzen et al. (2010) as predictor and the EIT as the predictand is computed to receive Ellenberg based UHI values (UHIE). Therefore, both UHI datasets are not fully independent. The UHIE dataset covers the area of the city of Hamburg on a $1 \times 1, \mathrm{km}^2$ grid, without water bodies, because floristic mapping data do not exist for water-covered areas. For the calculation of the spatial correlation, the UHI pattern simulated by METRAS is linearly interpolated onto the grid of the UHIE dataset.

For the 3 different observations (annual- and summer-averaged UHI from DWD measurements, UHIE dataset), the spatial correlation coefficient is calculated. All correlations are significant at $\alpha = 0.1$. The highest correlation with $r = 0.8$ is obtained for the comparison between the METRAS-1 km result (Figure 7) and the summer-averaged UHI followed by the annual averaged UHI ($r = 0.76$) and the UHIE ($r = 0.74$). The latter is significant at $\alpha = 0.05$ due to the larger sample.

Table 3: Spatial correlation coefficients determined for the comparison between the UHIE pattern derived by Bechtel and Schmidt (2011) and the UHI patterns for the different METRAS-1 km simulations. All values are statistically significant at $\alpha = 0.05$.

Simulation name	Correlation coefficient
WP1M	0.63
WP1T	0.49
WP2M	0.51
WP2T	0.61
WP3M	0.60
WP3T	0.51
WP4M	0.70
WP4T	0.36
WP5M	0.47
WP5T	0.48
WP6M	0.60
WP6T	0.61
WP7M	0.48

The comparison with observed data can be used to identify the simulation that shows the best agreement with observations (Table 2). For the comparison with the observed UHI (Schlünzen et al., 2010), no significant spatial correlations can be found for any single WP. Therefore, Table 3 lists only the spatial correlations for the different METRAS-1 km simulations in comparison with the UHIE dataset. All correlations are lower than the correlation between UHIE and the statistically recombined UHI pattern ($r = 0.74$). This shows that more than one simulation needs to be conducted to obtain an UHI that is close to the observations. The highest correlations ($r = 0.7$) can be found for the WP4M results. Therefore, this simulation could be used for sensitivity studies regarding adaption measures, if only the UHI pattern is of interest. The lowest value for the correlation is found for WP4T ($r = 0.37$). Hence, it cannot be concluded that WP4 generally produces a typical UHI pattern. The correlation coefficients for other simulations range from 0.47 to 0.63.

5.3 Future climate

Future changes in the statistical-dynamically downscaled average strong UHI pattern are determined by calculating the statistical weights (Eq. (2.6) and Eq. (2.7)) for both RCMs (CLM and REMO) for different periods. For the present climate, the period 1971–2000 is chosen. For the future climate, the two periods 2036–2065 and 2070–2099 are used. The two realizations of REMO and CLM projections are combined as done by Hoffmann and Schlünzen (2013). This accounts to some extent for the natural climate variability. Afterwards, the difference between the present average strong UHI pattern and the future average strong UHI pattern is calculated. Besides changes in the UHI pattern, the number of strong UHI days N_{strong} (Eq. 2.2) might change as well. Hence, the annual N_{strong} is calculated for present and future periods. The statistical significance of these changes is determined using bootstrap re-sampling (10000 resamples). The applied method accounts only for changes of the UHI due to changes in the climatology. Changes of the UHI due to changing urban morphology of Hamburg are not considered. For these simulations with the mesoscale model using different surface cover maps would be required.

Table 4: Annual number of strong UHI days N_{strong} ($\Delta T_{u-r} \geq 3$ K) in summer (JJA) for different RCM results and different periods. The two realizations of REMO and CLM are combined. Results are shown for non-corrected and bias-corrected projections of REMO and CLM. Significant changes ($\alpha = 0.05$) are indicated by (**).

period	REMO		CLM	
	without bias-correction	with bias-correction	without bias-correction	with bias-correction
1971–2000	16.3	22.2	10.2	24.6
2036–2065	16.9	22.8	11.4	26.8
2070–2099	17.3	26.8	15.4**	32.0**

For the RCM data without bias correction, the changes in the average strong UHI pattern for the future period 2036–2065 are presented in Fig. 8. For both REMO and CLM, the changes are marginal (Figs. 8a, b). They show slight increases within the city. These changes are, however, below 0.05 K. Even though the pattern does not change; N_{strong} slightly increases for both models (Table 4). These changes are not significant. N_{strong} is underestimated by REMO and CLM for the present climate without bias correction (ERA40 = 24.9 days). This is mostly due to biases in the variables used in the statistical model (Schoetter et al., 2012), which reduce the statistically modelled UHI. Hence, it is questionable if the statistical model, which is determined from observations, can be directly applied to uncorrected RCM results. For that reason, the bias-corrected RCM data (Section 3) are used to investigate the corresponding UHI changes. Figs. 8c, d show changes in the UHI pattern for the bias-corrected RCM data. REMO shows nearly no changes at all, while the UHI magnitude derived from CLM data increases almost constantly over large parts of the city as well as over the surrounding rural areas. With the bias correction REMO still underestimates N_{strong} by 2.7 days for the present climate while the CLM result is very close to the value derived from the combination of ERA40 based WPs and observation based statistical model results (Table 4). For REMO, the absolute signal remains constant with +0.7 days for 2036–2065. The signal for CLM increases to +2.2 days. Nevertheless, both change signals are not significant.

For 2070–2099, the changes for the uncorrected REMO and CLM results are smaller than for the earlier period (Figs. 9a, b). However, the number of strong UHI days increases about +1 day for the REMO results and up to +5.2 days for the CLM results. The latter increase is statistically significant. The area of the largest increases occurs over the river Elbe. This is due to in-

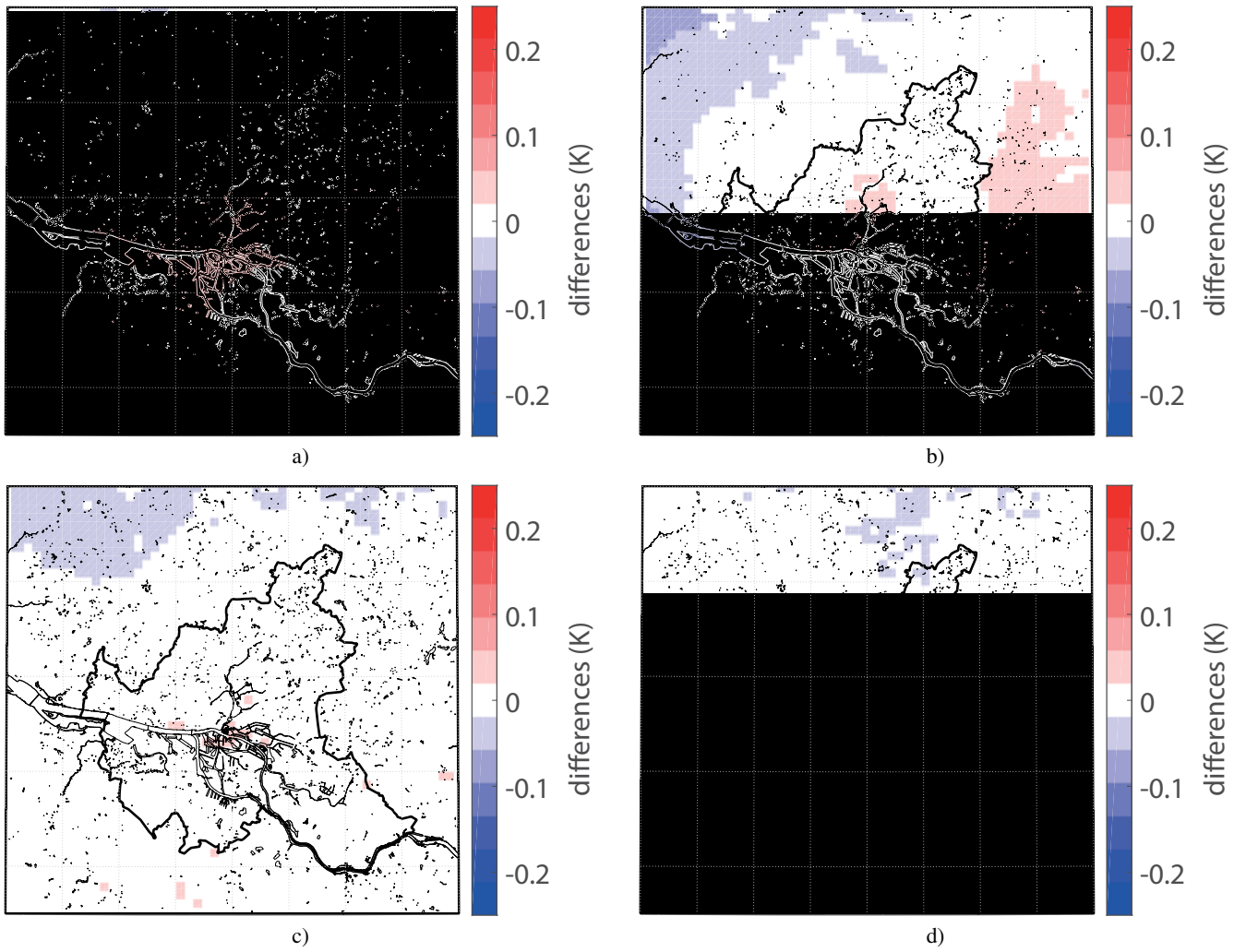

Figure 8: Differences in the statistically-dynamically downscaled average strong UHI pattern (8 p.m. to 12 a.m. LST) in summer (JJA) between the future period 2036–2065 and the present climate (1971–2000) using uncorrected (a) REMO and (b) CLM and bias-corrected (c) REMO and (d) CLM data.

creased weighting of simulations where the UHI pattern is strongly affected by water bodies (e.g. WP4M). The increases in the surroundings of Hamburg indicate that the changes can partly be attributed to non-urban related features of some simulations, for example an east-west temperature gradient over the whole domain.

Using the bias-corrected data, the changes are smaller for REMO (Fig. 9c). For CLM results, large changes in the UHI pattern (Fig. 9d) are found. In the western parts of Hamburg, the UHI increases up to 0.13 K. The bias correction also changes the signal of N_{strong} from +5.2 days to +7.2 days. After the bias correction, the increase of N_{strong} calculated based on REMO results increases from +1 day to +4.6 days, which is still not statistically significant.

6 Discussion

Since the presented downscaling method involves simulations of real (past) weather situations, these mesoscale model results can be directly evaluated with observed data. For both resolutions, the temperatures are underestimated while the relative humidity is overestimated. An influence of such biases on the UHI is possible and should be investigated in model sensitivity studies. From the 238 evaluation studies summarized by Schlünzen et al. (2015) 25 % have a bias below −1.1 K; thus the simulations conducted in the present study are on average well within the range of evaluation studies performed by other mesoscale models at similar horizontal resolution. The variation between the evaluation results of the individual simulations is, however, high, such that some simulations show results like the best evaluation results summarized by Schlünzen et al. (2015). Furthermore, the higher resolution improves the simulation of the near-surface flow field, which can be expected due to the better representation of the topography and surface cover. The differences in temperature and humidity between the two model setups might not only be due to the different resolution, but also to the different surface representation (Section 4.2). In addition to the number

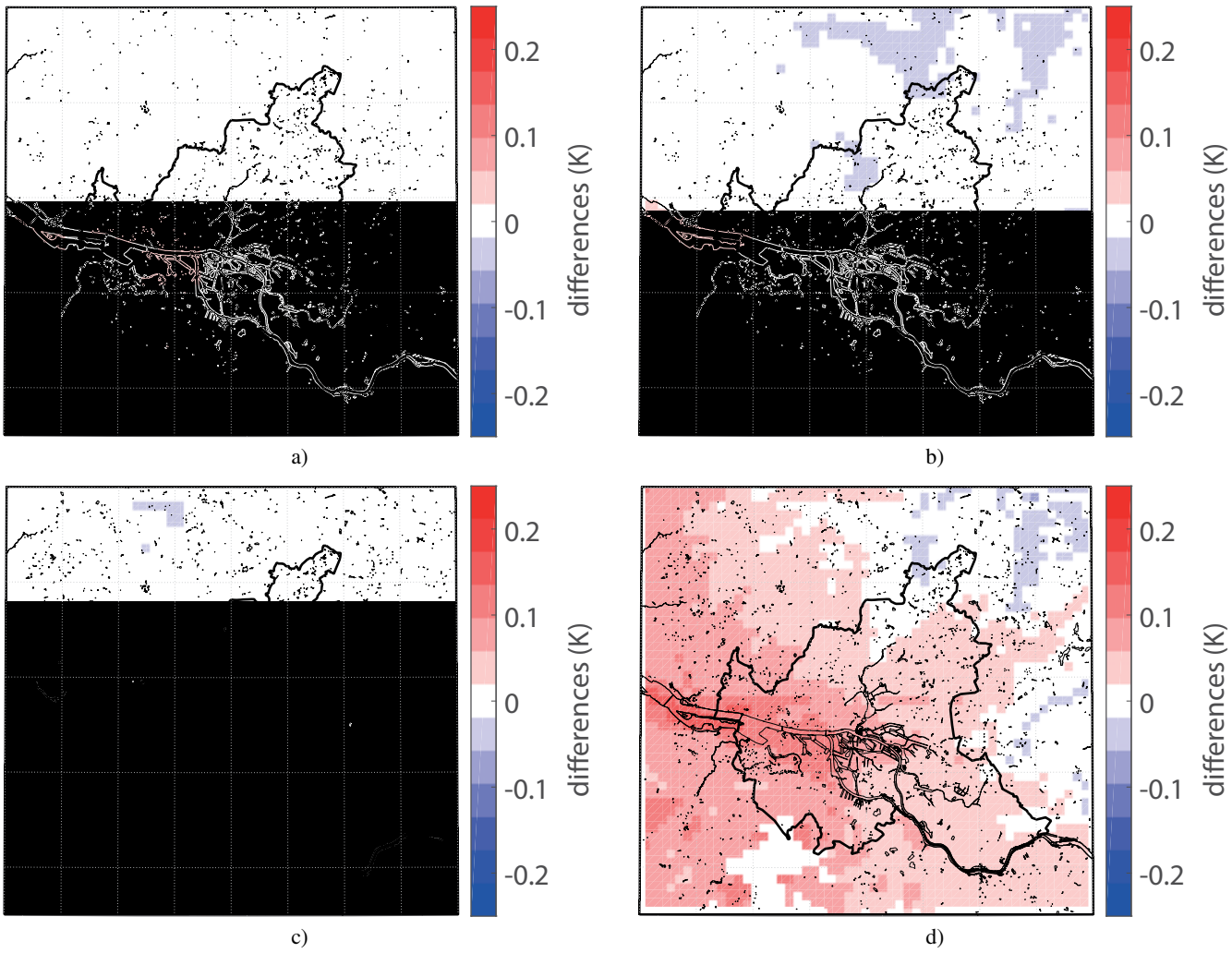

Figure 9: Differences in the statistically-dynamically downscaled average strong UHI pattern (8 p.m. to 12 a.m.) in summer (JJA) between the future period 2070–2099 and the present climate (1971–2000) using uncorrected (a) REMO and (b) CLM, bias-corrected (c) REMO and (d) CLM data.

of surface cover classes, the classes also differ in their respective parameters (Table 1). For instance, the land-use class "meadows" is split into four different classes of grass (short dry, long dry, short wet, and long wet) while none of them has the same parameter as "meadows". Urban areas are attributed to several typical urban classes (e.g. high and low buildings, asphalt) but also trees, bushes and grass are considered.

The simulated UHI intensity is lower than to be expected from the statistically modelled UHI. This inconsistency can be explained partially by the different definition used to calculate ΔT_{u-r}. The statistical model is based on differences in the minimum temperature (Section 2), while the temperature differences ΔT_{u-r} from the numerical simulations are calculated at a fixed time. Another reason is that the numerically simulated temperatures are average temperatures over an area of $1 \times 1\,\mathrm{km}^2$ which is sealed by 70 % at a maximum. The DWD station St. Pauli used for calculation of the "observed" strong UHI has been located in an area with rather high buildings with many sealed surfaces close by, which might therefore lead to the rather strong observed UHI. The other suburban sites in Hamburg show much lower UHI values (Schlünzen et al., 2010). Also the comparison of differences of simulated temperature in 10 m above ground with observed differences of temperature in 2 m above ground can lead to smaller UHI intensities. Flagg (2010), who conducted simulations for Detroit using the Weather Research and Forecast Model (WRF), showed that the urban-rural temperature differences in model results are larger when using the 2 m values instead of values in the lowest model level.

As shown in Section 4, the relative humidity is overestimated in most of the simulations. This could also lead to a reduction of the UHI because both variables are inversely related. Additionally, the lack of a canopy layer parameterization reduces the urban effect that accounts among others for radiative trapping in street canyons. METRAS simulations conducted for London using the Building Effect Parameterisation (BEP, Martilli et al., 2002) showed an increase of at most 1 K within urban areas compared to simulations without

BEP (Grawe et al., 2012). In addition, the effect of anthropogenic heat release is disregarded in the present study. Petrik et al. (2015) showed that for Hamburg, the nocturnal urban temperatures increase locally by up to 0.5 K when incorporating anthropogenic heat release. This is a local maximum value, which will be smaller at daytime (increased boundary layer height) and in summertime (reduced energy demand for heating). It additionally depends on the time of the day because the energy usage is usually reduced at night-time. The radiative trapping effect and the anthropogenic heat might not superimpose linearly, but including them would increase the simulated UHI intensity. Future studies should include additional scenarios for the anthropogenic heat emissions and study their impact on the UHI and in combination with the climate change. Also the variability of the 2 m temperature within a grid cell could be studied and a more detailed consideration of building effects be included. Information on buildings within Hamburg are now available (Schoetter et al., 2013).

The analysis of the statistically recombined UHI pattern shows that the maximum UHI intensity (~1.2 K) is located in the inner parts of the city, including harbour areas, which agrees well with the UHIE. The UHI pattern is largely affected by water surfaces. Hence, water temperatures seem to be crucial when simulating the local climate for Hamburg. At the moment river temperatures are set using interpolated SST data. In further studies measured river temperature data from the Wassergütemessnetz (WGMN) could be used (Fock, 2014). Anthropogenic heat emissions should also be considered in an additional scenario study, since water temperatures in lakes and rivers are also affected by human activities, e.g. usage of river water for the cooling of power plants. The SDD method also assumes that the difference between water temperature and air temperature remains unchanged in the future climate. To verify this, a river model should be coupled with transient RCM projections, which should also consider the mentioned anthropogenic effects.

Despite the above mentioned shortcomings the simulated pattern of Hamburg's UHI is quite well represented when compared to the available observations. This proves the usefulness of the SDD method to simulate the UHI. In addition, the representation of the urban surfaces in METRAS is sufficient to study urban effects.

The employed observational data have some shortcomings, too. The DWD dataset has only a few urban stations; most of them are not operated anymore. In the next few years new long-term urban climate measurements from the Hamburg Urban Soil Climate Observatory (HUSCO, Wiesner et al., 2014) will be available. This will substantially improve the understanding of Hamburg's UHI as well as help to improve the treatment of urban areas in METRAS.

Nonetheless, even with only 13 3-day simulations the SDD method is able to achieve a robust summer UHI pattern. This is a reduction of ~ 99 percent of the days that need to be simulated (13×3 days = 39 days instead of 30×92 days = 2760 days). But it has to be kept in mind that the pattern is just representative for strong UHI days (~25 % of summer days). This corresponds to a reduction of about ~ 94 %, which is still large. The reduction of the computational effort due to the SDD method is even higher when future changes are investigated because no additional simulations need to be conducted.

The future UHI is computed by applying the SDD method to regional climate projections from different RCMs. Thereby it is assumed that the morphology of the city does not change in a future climate. Since this will not be the case, a projection of the future surface cover should be considered, resulting in additional scenarios. Daneke (2013) developed a model for land-use changes in the greater city of Hamburg. With the projected land-use converted to the METRAS surface cover classes, the UHI changes can be determined with consideration of morphological changes (Boettcher et al., in review).

The UHI changes are determined for two 30-year periods. For the period 2036–2065, the changes in the UHI pattern as well as changes in the number of strong UHI days are not significant compared to 1971–2000 based on the REMO and CLM projections. However, both models show biases in the statistically modelled UHI for the current climate due to biases in the RCM variables. These biases are partially eliminated by the bias correction described in Schoetter et al. (2012). This bias correction is applied for all values within each month. However, it is not clear if the model biases are similar for different WPs. If this is not the case, the biases would need to be corrected for each WP separately. The change in the UHI pattern is only slightly influenced by the bias correction. However, the number of strong UHI days is increased by +1 day for CLM. The changes in the signal can be expected since threshold based variables are sensitive to a change in the statistical distribution. For 2070–2099, the bias-corrected CLM results show an increase in the western parts of Hamburg by up to 0.13 K. This corresponds to about 10 % of the simulated maximum UHI intensity (1.2 K) and is in the order of changes found by Hamdi et al. (2015) for Brussels and Paris for the summer season. However, they find a decrease of the UHI magnitude instead of an increase. For the uncorrected CLM results as well as for the REMO results the changes are small. The results also indicate that the pattern of the changes is affected by non-urban effects of individual simulations such as large-scale temperature gradients, probably due to the small number of simulations (13). The increase in the UHI intensity in CLM is caused by an increase of UHI values within WP4 (large meridional pressure gradient and advection of dry air masses) and an increase in the frequency of WP4. Hoffmann and Schlünzen (2013) showed that the frequency of WP4 increases especially at the end of the century in the CLM simulations. This is not the case for the uncorrected CLM results. The number of strong UHI days in CLM increases significantly by up to 5. This is mainly due to the reduction in the daily

relative humidity projected by this RCM (not shown). The increase of 3.6 days for REMO is not significant. Nevertheless, together with the findings of Hoffmann et al. (2012), who showed that the number of days with an UHI larger than 4 K increase significantly, the results point to occurrences of more strong UHI days in summer at the end of the 21st century.

7 Conclusions

A statistical-dynamical downscaling (SDD) method is developed and applied to downscale Hamburg's UHI. It combines a WPC with a statistical model for the UHI intensity to determine relevant weather situations, which are simulated with the mesoscale numerical model METRAS forced with ECMWF data. The final horizontal resolution of 1 km is achieved with a two-step nesting with an intermediate simulation on a 4 km grid. The 1 km simulations are conducted with a much more detailed surface cover classification that accounts for the heterogeneity of surfaces within the city. The UHI pattern is computed by a statistical recombination of the simulation results for different weather situations.

The main advantages of this method with respect to dynamical downscaling are the drastically reduced computational effort (~ 94 % for current climate) and the opportunity to evaluate not just one resulting UHI pattern but also the dynamical simulations because past weather situations are downscaled. The latter is also an advantage over the SDD method of Früh et al. (2011a,b), which simulated only idealized weather situations without nesting. The evaluation showed that METRAS performed well compared to other mesoscale modelling studies for most of the investigated variables. The resulting UHI pattern for the current climate corresponds well with the available observations, while the intensity is underestimated possibly due to the resolution, which might be still to coarse to correctly represent the heterogeneity of urban areas, and due to missing urban related effects in METRAS (i.e. anthropogenic heat release, radiative trapping). The highest UHI intensity was simulated in the densely build inner city of Hamburg and the harbour areas. Increased temperatures along the Elbe river indicate an important role of water bodies on night-time temperatures in Hamburg.

Applying the method to SRES A1B projections from the RCMs REMO and CLM does not give a coherent change signal in the UHI pattern. CLM shows an intensification of the averaged UHI in the western parts of the city for the end of the 21st century, while REMO shows no changes. However, the results show that there is a tendency towards more strong UHI days especially towards the end of the century. Consequently, climate adaptation measures need to be developed that reduce the UHI intensity to compensate some of the night-time temperature increases in Hamburg due to climate change.

In the present study the urban area structure of the city did not change. Therefore, urban development scenarios should be considered (e.g. Boettcher et al., in review), which will increase the number of high-resolution (1 km) simulations by a factor of two for each development scenario.

The present study shows that the proposed SDD method can help to investigate future changes in urban climate with a limited amount of computation resources. The small number of days that needs to be simulated means that the simulations could be downscaled further with high-resolution meso- or mircroscale models. In addition, it can be applied as a tool to investigate climate adaptation measures as well as climate mitigation measures (Boettcher et al., in review) for urban areas.

Acknowledgments

This work has been performed in the framework of the project KLIMZUG-NORD funded under grant 01LR0805D by the German Federal Ministry of Education and Research and supported in parts through the Cluster of Excellence "CliSAP" (EXC177), University of Hamburg, funded through the German Science Foundation (DFG).

The mesoscale model simulations have been conducted using the resources of the DKRZ supercomputer, contingent of the University of Hamburg.

The ERA 40 reanalysis data, the ERA Interim reanalysis data and the climate model data as well as climate model results have been downloaded from the "World Data Center for Climate" database (http://cera-www.dkrz.de).

Surface cover data and information on building characteristics have been retrieved from the "Freie und Hansestadt Hamburg, Landesbetrieb Geoinformation und Vermessung (Nr. 102156)", the "Landesamt für Geoinformation und Landentwicklung Niedersachsen (LGN)", the "Landesvermessungsamt Schleswig Holstein", the "Amt für Geoinformation" and the "Vermessungs- und Katasterwesen Mecklenburg Vorpommern". Costs for these datasets have been covered by the University of Hamburg as well as by the excellence cluster CliSAP.

References

Atkinson, B.W., 2003: Numerical modelling of urban heat-island intensity. – Bound.-Layer Meteorol. **109**, 285–310.

Augustin, W., V. Heuveline, G. Meschkat, K.H. Schlünzen, G. Schroeder, 2008: Open MP parallelization of the METRAS meteorology model: Application to the America's Cup. – Springer Berlin Heidelberg, High Performance Computing in Science and Engineering, Springer-Verlag, Berlin, Germany: 547–559.

Bechtel, B., K.J. Schmidt, 2011: Floristic mapping data as a new proxy for the mean urban heat island. – Climate Res. **49**, 45–58, DOI:10.3354/cr01009.

Boé, J., L. Terray, 2008: A Weather-Type Approach to Analyzing Winter Precipitation in France: Twentieth-Century Trends and the Role of Anthropogenic Forcing. – J. Climate **21**, 3118–3133.

Boé, J., L. Terray, F. Habets, E. Martin, 2006: A simple statistical-dynamical downscaling scheme based on weather types and conditional resampling. – J. Geophys. Res. **111**, D23106, DOI:10.1029/2005JD006889.

Boettcher, M., P. Hoffmann, H.J. Lenhart, K.H. Schlünzen, R. Schoetter, 2015: Influence of large offshore wind farms on North German climate. – Meteorol. Z. 24, 465–480, DOI:10.1127/metz/2015/0652.

Boettcher, M., D.D. Flagg, D. Grawe, P. Hoffmann, R. Petrik, K.H. Schlünzen, R. Schoetter, N. Teichert, in review: Modelling impacts of urban developments and climate adaptation measures on summer climate of Hamburg. – Urban Climate.

Bohnenstengel, S.I., 2011: Can a simple locality index be used to improve mesoscale model forecasts? – Department Geowissenschaften, Universität Hamburg. Ph.D. thesis.

Bohnenstengel, S.I., S. Evans, P.A. Clark, S. Belcher, 2011: Simulations of the London urban heat island. – Quart. J. Roy. Meteor. Soc. **137**, 1625–1640, DOI:10.1002/qj.855.

Brutsaert, W., 1972. Radiation, evaporation and the maintenance of turbulence under stable conditions in the lower atmosphere. – Bound.-Layer Meteor. **2**, 309–325.

Buschbom, J., S. Gimmerthal, P. Kirschner, I.M. Michalczyk, Sebbenn, S. Schueler, K.H. Schlünzen, B. Degen, 2012: Spatial composition of pollen-mediated gene flow in sessile oak. – Archive Forest Sci. **83**, 12–18.

Bungert, U., 2008: Einfluss der Nestung auf die Ergebnisse meteorologischer Modelle. – Ph.D. thesis, Dept. Geowissenschaften, Universität Hamburg: 134 pp.

Cassou, C., M. Minvielle, L. Terray, C. Périgaud, 2011: A statistical-dynamical scheme for reconstructing ocean forcing in the Atlantic. Part I: weather regimes as predictors for ocean surface variables. – Climate Dyn. **36**, 19–39, DOI: 10.1007/s00382-010-0781-7.

Claussen, M., 1991: Estimation of areally-averaged surface fluxes. Bound.-Layer Metorol.54: 387–410.

Cox, R, B.L. Bauer, T. Smith, 1998: A mesoscale model intercomparison. – Bull. Amer. Meteor. Soc.**79**, 265–283, DOI: 10.1175/1520-0450(1981)020<0203:AACC>2.0.CO;2.

Daneke, C., 2013: Modellierung von Stadtentwicklungsprozessen am Beispiel Hamburgs unter Berücksichtigung stadtklimatologischer Aspekte. – Dissertation zur Erlangung des Doktorgrades der Naturwissenschaften im Fachbereich Geographie der Universität Hamburg, 211 pp.

Daschkeit, A., 2011: Das Klima der Region und mögliche Entwicklungen in der Zukunft bis 2100. – In: von Storch H., M. Claussen (Hrsg.): Klimabericht für die Metropolregion Hamburg, 61–90, DOI:10.1007/978-3-642-16035-6.

Deardorff, J.W., 1978: Efficient prediction of ground surface temperature and moisture, with inclusion of a layer of vegetation. – J. Geophys. Res.-Atmos. **83**, 1889–1903.

Dee, D.P., S.M. Uppala, A.J. Simmons, P. Berrisford, P. Poli, S. Kobayashi, U. Andrae, M.A. Balmaseda, G. Balsamo, P. Bauer, P. Bechtold, A.C.M. Beljaars, L. van de Berg, J. Bidlot, N. Bormann, C. Delsol, R. Dragani, M. Fuentes, A.J. Geer, L. Haimberger, S.B. Healy, H. Hersbach, E.V. Hólm, L. Isaksen, P. Kållberg, M. Köhler, M. Matricardi, A.P. McNally, B.M. Monge-Sanz, J.-J. Morcrette, B.-K. Park, C. Peubey, P. de Rosnay, C. Tavolato, J.-N. Thépaut, F. Vitart, 2011: The ERA-Interim reanalysis: configuration and performance of the data assimilation system. – Quart. J. Roy. Meteor. Soc. **137**, 553–597, DOI:10.1002/qj.828.

Demuzere, M., M. Werner, N.P.M. van Lipzig, E. Roeckner, 2009: An analysis of present and future ECHAM5 pressure fields using a classification of circulation patterns. – Int. J. Climatol. **29**, 1796–1810.

Dierer, S., K.H. Schlünzen, 2005: Influence parameters for a polar mesocyclone development. – Meteorol. Z. **14**, 781–792.

ECMWF, 2009: PART II: DATA ASSIMILATION. IFS DOCUMENTATION. – Cy33r1 Operational implementation 3 June 2008: 160 pp.

ECMWF, 2010: PART II: DATA ASSIMILATION. IFS DOCUMENTATION. – Cy36r1 Operational implementation 26 January 2010: 168 pp.

Flagg, D.D., 2010: Mesoscale modeling of the urban boundary layer in a coastal environment. – Ph.D. thesis, York University, Toronto, Ontario: 250 pp.

Flagg, D.D., R. Schoetter, M. Linde, P. Kirschner, D. Grawe, K.H. Schluenzen, 2011: Development of surface cover classes for the M-SYS models from land-use land-cover datasets. – CLiSAP D4 Workshop, University of Hamburg, Hamburg, Germany. 17 November 2011.

Fock, B.H., 2014: RANS versus LES models for investigations of the urban climate. – Ph.D. thesis, Department Geowissenschaften, Universität Hamburg.

Frey-Buness, F, D. Heimann, R. Sausen, 1995: A statistical-dynamical downscaling procedure for global climate simulations. – Theo. Appl. Climatol. **50**, 117–131.

Früh, B., P. Becker, T. Deutschländer, J.-D. Hessel, M. Kossmann, I. Mieskes, J. Namyslo, M. Roos, U. Sievers, T. Steigerwald, H. Turau, U. Wienert, 2011a: Estimation of Climate-Change Impacts on the Urban Heat Load Using an Urban Climate Model and Regional Climate Projections. – J. Appl. Meteor. Climatol. **50**, 167–184.

Früh, B, M. Kossmann, M. Roos, 2011b: Frankfurt am Main im Klimawandel – Eine Untersuchung zur städtischen Wärmebelastung. – Berichte des Deutschen Wetterdienstes **237**, 68 pp.

Fuentes, U., D. Heimann, 2000: An improved statistical-dynamical downscaling scheme and its application to the Alpine precipitation climatology. – Theor. Appl. Climatol. **65**, 119–135.

Grawe, D., H.L. Thompson, J.A. Salmond, X.M. Cai, K.H. Schlünzen, 2012: Modelling the impact of urbanisation on regional climate in the Greater London Area. – Int. J. Climatol. **33**, 2388–2401. DOI:10.1002/joc.3589.

Hafner, J., S.Q. Kidder, 1999: Urban heat island modeling in conjunction with satellite-derived surface/soil parameters. – J. Appl. Meteor. **38**, 448–465.

Hamdi, R., H. Van de Vyver, R. De Troch, P. Termonia, 2014: Assessment of three dynamical urban climate downscaling methods: Brussels's future urban heat island under an A1B emission scenario. – Int. J. Climatol., **34**, 978–999. DOI: 10.1002/joc.3734.

Hamdi, R., O. Giot, R. De Troch, A. Deckmyn, P. Termonia, 2015: Future climate of Brussels and Paris for the 2050s under the A1B scenario. – Urban Climate, **12**, 160–182, DOI: 10.1016/j.uclim.2015.03.003.

Hebbinghaus, H., S. Dierer, K.H. Schlünzen, 2007: Sensitivity studies on vortex development over a polynya. – Theo. Appl. Climatol. **88**, 1–16, DOI:10.1007/s00704-006-0233-9.

Herbert, F., G. Kramm, 1985: Trockene Deposition reaktionsträger Substanzen, beschrieben mit einem diagnostischen Modell der bodennahen Luftschicht. In: Beder K.H., G. Löbel (Eds): Atmosphärische Spurenstoffe und ihr physikalisch-chemisches Verhalten. – Springer Verlag, Berlin, 264 pp.

Hjemfelt, M.R., 1982: Numerical simulation of the effects of St. Louis on mesoscale boundary layer airflow and vertical motion: Simulations of urban vs. non-urban effects. – J. Appl. Meteor. **21**, 1239–1257.

Hoffmann, P., 2012: Quantifying the influence of climate change on the urban heat island of Hamburg using different downscaling methods. – Ph.D. thesis, Department Geowis-

senschaften, University of Hamburg, 130 pp. http://ediss.sub.uni-hamburg.de/volltexte/2012/5716/

Hoffmann, P., K.H. Schlünzen, 2013: Weather pattern classification to represent the urban heat island in present and future climate. Journal of Applied Meteorology and Climatology, **52**, 2699–2714. DOI:10.1175/JAMC-D-12-065.1.

Hoffmann, P., O. Krueger, K.H. Schlünzen, 2012: A statistical model for the urban heat island and its application to a climate change scenario. – Int. J. Climatol, **32**, 1238–1248. DOI:10.1002/joc.2348.

Hollweg, H.-D., U. Böhm, I. Fast, B. Hennemuth, K. Keuler, E. Keup-Thiel, M. Lautenschlager, S. Legutke, K. Radtke, B. Rockel, M. Schubert, A. Will, M. Woldt, C. Wunram, 2008: Ensemble simulations over Europe with the regional climate model CLM forced with IPCC AR4 global scenarios. – M & D Technical Report **3**, 154 pp.

Huebener, H., M. Kerschgens, 2007a: Downscaling of current and future rainfall climatologies for southern Morocco. Part I: Downscaling method and current climatology. – Int. J. Climatol. **27**, 1763–1774.

Huebener, H., M. Kerschgens, 2007b: Downscaling of current and future rainfall climatologies for southern Morocco. Part II: Climate change signals. – Int. J. Climatol. **27**, 1065–1073.

Jacob, D., 2001: A note to the simulation of the annual and inter-annual variability of the water budget over the Baltic Sea drainage basin. – Meteor. Atmos. Phys. **77**, 61–73.

Jacob, D., R. Podzun, 1997: Sensitivity studies with the regional climate model REMO. – Meteor. Atmos. Phys. **63**, 119–129.

Jacob, D., B.J.J.M. Van den Hurk, U. Andrae, G. Elgered, C. Fortelius, L.P. Graham, S.D. Jackson, U. Karstens, C. Koepken, R. Lindau, R. Podzun, B. Rockel, F. Rubel, B.H. Sass, R. Smith, X. Yang, 2001: A Comprehensive Model Intercomparison Study Investigating the Water Budget During the PIDCAP Period. – Meteor. Atmos. Phys. **77**, 19–43.

Jacob, D., H. Göttel, S. Kotlarski, P. Lorenz, K. Sieck, 2008. Klimaauswirkungen und Anpassung in Deutschland Phase 1: Erstellung regionaler Klimaszenarien für Deutschland. – Abschlussbericht zum UFOPLAN-Vorhaben 204 41 13, 154 pp.

Jungclaus, J.H., M. Botzet, H. Haak, N. Keenlyside, M. Latif, J. Marotzke, U. Mikolajewicz, E Roeckner, 2006: Ocean circulation and tropical variability in the model ECHAM5/MPI-OM. – J. Climate **19**, 3952–3972.

Katzfey, J.J., K.C. Nguyen, J. McGregor, P. Hoffmann, S. Ramasamy, H.T. Nguyen, H.V. Nguyen, K.V. Mai, T.V. Nguyen, K.T. Ba, T.V. Van, T.V. Phan, T.Q. Nguyen, N.D. Thanh, L.T. Trinh, 2016: High-resolution projections for Vietnam – Methodology and evaluation for current climate. Asia-Pacific J. Atmos. Sci. **52**, 91–106, DOI: 10.1007/s13143-016-0011-2

Kessler, E., 1969: On the distribution and continuity of water substance in atmospheric circulatio –Meteor. Monogr. **32**, Amer. Meteor. Soc., Boston, 81 pp.

Kim, Y.-H., J-J Baik, 2002: Maximum urban heat island intensity in Seoul. – J. Appl. Meteorol. **41**, 651–659.

Kim, Y.-H., J-J Baik, 2004: Daily maximum urban heat island intensity in large cities of Korea. Theor. Appl. Climatol. **79**, 151–164, DOI:10.1007/s00704-004-0070-7.

Lengfeld, K. 2012: Assessing Near Surface Variability with a Wireless Sensor Network on the Small Scale. – Ph.D. thesis, Department Geowissenschaften, Universität Hamburg: 131 pp.

Lengfeld, K, F. Ament, 2012: Observing local-scale variability of near-surface temperature and humidity using a wireless sensor network. – J. Appl. Meteor. Climatol. **51**, 30–41, DOI: 10.1175/JAMC-D-11-025.1.

Lüpkes, C., K.H. Schlünzen, 1996: Modelling the Arctic convective boundary-layer with different turbulence parameterizations. – Bound.-Layer Meteor. **79**, 107–130.

Lüpkes, C., T. Vihma, G. Birnbaum, U. Wacker, 2008: Influence of leads in sea ice on the temperature of the atmospheric boundary layer during polar night. – Geophys. Res. Lett. **35**, L03805.

Martilli, A., A. Clappier, M.W. Rotach, 2002: An Urban Surface Exchange Parameterisation for Mesoscale Models. – Bound.-Layer Meteor. **104**, 261–304.

Masson, V., 2000: A physically-based scheme for the urban energy budget in atmospheric models. – Bound.-Layer Meteor. **94**, 357–397.

Mesinger, F., A. Arakawa, 1976: Numerical methods used in atmospheric models. – Garp Publications Series No. **17**, Volume I, 64 pp.

Morris, C.J.G., I. Simmonds, N. Plummer, 2001: Quantification of the influences of wind and cloud on the nocturnal urban heat island of a large city. – J. Appl. Meteor. **40**, 169–182.

Najac, J., C. Lac, L. Terray, 2011: Impact of climate change on surface winds in France using a statistical-dynamical downscaling method with mesoscale modelling. – Int. J. Climatol. **31**, 415–430. DOI:10.1002/joc.2075.

Niemeier, U., K.H. Schlünzen, 1993: Modelling steep terrain influences on flow patterns at the Isle of Helgoland. – Beitr. Phys. Atmos. **66**, 45–62.

Oke, TR., 1987: Boundary layer climates. 2nd Edition. – Routledge, Taylor and Francis Group, Cambridge, 435 pp.

Petrik, R., D. Grawe, K.H. Schlünzen 2015: Investigating the impact of anthropogenic heat on urban climate using a top-down methodology. – 9th International Conference on Urban Climate, Toulouse, France, 20.7.2015, http://www.meteo.fr/icuc9/presentations/UCP/UCP2-2.pdf.

Philipp, A., J. Jacobait, D.R. Fereday, P.D. Jones, A. Moberg, H. Wanner, 2007: Long-term variability of daily North Atlantic–European pressure patterns since 1850 classified by simulated annealing clustering. – J. Climate **20**, 4065–4095.

Piani, C., J.O. Haerter, E. Coppola, 2010: Statistical bias correction for daily precipitation in regional climate models over Europe. – Theor. Appl. Climatol. **99**, 187–192.

Pinto, J.G., C.P. Neuhaus, G.C. Leckebusch, M. Reyers, M. Kerschgens, 2010: Estimation of wind storm impacts over West Germany under future climate conditions using a statistical-dynamical downscaling approach. – Tellus **A62**: 188–201, DOI:10.1111/j.1600-0870.2009.00424.x.

Renner, E., A. Münzenberg, 2003: Impact of biogenic terpene emissions from Brassica napus on tropospheric ozone over Saxony (Germany) – Num. Invest. Env. Sci. Poll. Res. **10**, 147–153. DOI:10.1065/espr2003.05.154.

Reynolds, R.W., N.A. Rayner, T.M. Smith, D.C. Stokes, W. Wang, 2002: An improved in situ and satellite SST analysis for climate. – J. Climate **15**, 1609–1625.

Ries, H., K.H. Schlünzen, 2009: Evaluation of a mesoscale model with different surface parameterizations and vertical resolutions for the bay of Valencia. – Mon. Wea. Rev. **137**, 2646–2661, DOI:10.1175/2009MWR2836.1.

Ries, H, K.H. Schlünzen, B. Brümmer, M. Claussen, G. Müller, 2010: Impact of surface parameter uncertainties on the development of a trough in the Fram Strait region. – Tellus **62A**, 377–392. DOI:10.3402/tellusa.v62i4.15704.

Roeckner, E., G. Bäuml, L. Bonaventura, R. Brokopf, M. Esch, M. Giorgetta, S. Hagemann, I. Kirchner, L. Kornblueh, E. Manzini, A. Rhodin, U. Schlese, U. Schulzweida, A. Tompkins, 2003: The atmospheric general circulation model ECHAM 5. PART I: Model description. – Max-Planck-Institute for Meteorology, Hamburg, 127 pp.

Schlünzen, K.H., 1990: On the inland penetration of sea breeze fronts. – Beitr. Phys. Atmos. **63**, 243–256.

Schlünzen, K.H., 1992: Modellierung des Strömungsfeldes über Norddeutschland für den 23.Mai 1989. – Ann. Meteor. NF **27**, 308–309.

Schlünzen, K.H., J.J. Katzfey, 2003: Relevance of sub-grid-scale land-use effects for mesoscale models. – Tellus **55A**: 232–246.

Schlünzen, K.H., E.M.I. Meyer, 2007: Impacts of meteorological situations and chemical reactions on daily dry deposition of nitrogen into the Southern North Sea. – Atmos. Env. **41**, 289–302.

Schlünzen, K.H., R.S. Sokhi, 2008: Overview of tools and methods for meteorological and air pollution mesocale model evaluation and user training. – GAW Report No. 181, WMO/TD-No. 1457, 116 pp.

Schlünzen, K.H., P. Hoffmann, G. Rosenhagen, W. Riecke, 2010: Long-term changes and regional differences in temperature and precipitation in the metropolitan area of Hamburg. – Int. J. Climatol. **30**, 1121–1136, DOI:10.1002/joc.1968.

Schlünzen, K.H., D. Grawe, S.I. Bohnenstengel, I. Schlüter, R. Koppmann, 2011: Joint modelling of obstacle induced and mesoscale changes – current limits and challenges. – J. Wind Eng. Ind. Aerodyn. **99**, 217–255, DOI: 10.1016/j.jweia.2011.01.009.

Schlünzen, K.H., D.D. Flagg, B.H. Fock, A. Gierisch, C. Lüpkes, V. Reinhardt, C. Spensberger, 2012a: Scientific Documentation of the Multiscale Model Sy4stem M-SYS (METRAS, MITRAS, MECTM, MICTM, MESIM). – MEMI Technical Report **4**, 138 pp.

Schlünzen, K.H., U. Bungert, D.D. Flagg, B.H. Fock, A. Gierisch, D. Grawe, P. Kirschner, C. Lüpkes, V. Reinhardt, H. Ries, R. Schoetter, C. Spensberger, M. Uphoff, 2012b: Technical Documentation of the Multiscale Model System M-SYS (METRAS, MITRAS, MECTM, MICTM, MESIM). – MEMI Technical Report **3**, 138 pp.

Schlünzen, K.H., K. Conrady, C. Purr, 2015: Typical performances of mesoscale meteorology models. – In Steyn, D.G., H. Chaumerliac (Eds.): Air Pollution Modeling and its Application XXIV. – Berlin, Springer. DOI: 10.1007/978-3-319-24478-5_72; p 447-457.

Schoetter, R., P. Hoffmann, D. Rechid, K.H. Schlünzen, 2012: Evaluation and bias correction of regional climate model results using model evaluation measures. – J. Appl. Meteor. Climatol. **51**, 1670–1684.

Schoetter, R., D. Grawe, P. Hoffmann, P. Kirschner, A. Gratz, K.H. Schlünzen, 2013: Impact of local adaptation measures and regional climate change on perceived temperature. – Meteorol. Z. **22**, 117–130.

Schüler, S., K.H. Schlünzen, 2006: Modeling of oak pollen dispersal on the landscape level with a mesoscale atmospheric model. – Env. Model Assess. **11**, 179–194. DOI: 10.1007/s10666-006-9044-8.

Sheng, L., K.H. Schlünzen, Z. Wu, 2000: Three-dimensional numerical simulation of the mesoscale wind structure over Shandong peninsula. – Acta Meteorol. Sinica **1**, 9–107.

Thompson, H.L., 2008: Modelling the impact of urbanisation on the region of the Greater London Area. – PhD thesis, School of Geography, The University of Birmingham, Birmingham, UK, 263 pp.

Uppala, S.M., P.W. Kallberg, A.J. Simmons, U. Andrae, V.D. Bechtold, M. Fiorino, J.K. Gibson, J. Haseler, A. Hernandez, G.A. Kelly, X. Li, K. Onogi, S. Saarinen, N. Sokka, R.P. Allan, E. Andersson, K. Arpe, M.A. Balmaseda, A.C.M. Beljaars, L. Van De Berg, J. Bidlot, N. Bormann, S. Caires, F. Chevallier, A. Dethof, M. Dragosavac, M. Fisher, M. Fuentes, S. Hagemann, E. Holm, B.J. Hoskins, L. Isaksen, P.A.E.M. Janssen, R. Jenne, A.P. McNally, J.F. Mahfouf, J.J. Morcrette, N.A. Rayner, R.W. Saunders, P. Simon, A. Sterl, K.E. Trenberth, A. Untch, D. Vasiljevic, P. Viterbo, J. Woollen, 2005: The ERA 40 re-analysis. – Quart. J. Roy. Meteor. Soc. **131**, 2961–3012.

von Salzen, K., M. Claussen, K.H. Schlünzen, 1996: Application of the concept of blending height to the calculation of surface fluxes in a mesoscale model. – Meteorol. Z. **5**, 60–66.

Wiesner, S., A. Eschenbach, F. Ament, 2014: Urban air temperature anomalies and their relation to soil moisture observed in the city of Hamburg. – Meteorol. Z. **23**, 143–157. DOI: 10.1127/0941-2948/2014/0571.

Wilby, R.L., 2003: Past and projected trends in London's urban heat island. – Weather **58**, 251–260.

Wilby, R.L., 2008: Constructing climate change scenarios of urban heat island intensity and air quality. – Env. Planning B: Planning and Design **35**, 902–919.

Wilby, R.L., T.M.L. Wigley, 1997: Downscaling general circulation model output: a review of methods and limitations. – Progr. Phys. Geogr. **21**, 530–548.

Wu, Z., K.H. Schlünzen, 1992: Numerical study on the local wind structures forced by the complex terrain of Qingdao area. – Acta Meteorol. Sinica **6**, 355–366.

Yow, D.M., 2007: Urban heat islands: Observations, impacts, and adaptation. – Geography Compass **1/6**, 1227–1251.

Zhou, Y., J.M. Shepherd, 2009: Atlanta's urban heat island under extreme heat conditions and potential mitigation strategies. – Nat. Hazards **52**, 639–668.